European Journal of Medicinal Chemistry 84 (2014) 343–363

Contents lists available at ScienceDirect

European Journal of Medicinal Chemistry

journal homepage: http://www.elsevier.com/locate/ejmech

Original article

Potentially bioactive organotin(IV) compounds: Synthesis, characterization, *in vitro* bioactivities and interaction with SS-DNA

Muhammad Sirajuddin [a], Saqib Ali [a, *], Vickie McKee [b], Manzar Sohail [c], Hammad Pasha [d]

[a] Department of Chemistry, Quaid-i-Azam University, Islamabad 45320, Pakistan
[b] Department of Chemistry, Loughborough University, Loughborough, Leics LE11 3TU, UK
[c] Center of Excellence for Nanotechnology, King Fahd University of Petroleum and Minerals, Dhahran 31261, Saudi Arabia
[d] Department of Biochemistry, Quaid-i-Azam University, Islamabad 45320, Pakistan

ARTICLE INFO

Article history:
Received 14 December 2013
Received in revised form
1 July 2014
Accepted 8 July 2014
Available online 9 July 2014

Keywords:
Organotin(IV) compound
DNA interaction
Antitumor activity
Antimicrobial activity
Cytotoxicity
Antileishmanial activity

ABSTRACT

Fourteen new organotin(IV) complexes with general formula R_2SnL_2 or R_3SnL where R = CH_3, C_2H_5, C_4H_9, C_6H_5, C_6H_{11}, $CH_2{-}C_6H_5$, $C(CH_3)_3$, C_8H_{17} and L = N-[(2-methoxyphenyl)]-4-oxo-4-[oxy]butanamide were synthesized and characterized by elemental analyses, FT-IR, NMR (^{1}H, ^{13}C and ^{119}Sn), mass spectrometry and single crystal X-ray structural analysis. Crystallographic data for four triorganotin(IV) complexes (R_3SnL, R = CH_3, C_2H_5, C_4H_9, $CH_2{-}C_6H_5$) showed the tin has approximate trigonal bipyramidal geometry with the R groups in the trigonal plane. The carboxylate groups of ligands L bridge adjacent tin atoms, resulting in polymeric chains. In case of the diorganotin(IV) derivatives a six-coordinate geometry at the tin atom is proposed from spectroscopic evidence. The Me–Sn–Me bond angle in complex **7** was determined from the $^2J[^{119}Sn{-}^1H]$ value as 166.3° that falls in the range of six-coordinate geometry. The ligand and its complexes (**1**–**14**) were screened for their antimicrobial, antitumor, cytotoxic and antileishmanial activities and found to be biologically active. The ligand and its complexes bind to DNA *via* intercalative interactions resulting in hypochromism and minor bathochromic shifts as confirmed by UV–visible spectroscopy. Based on *in vitro* studies such as the potato disc method, the synthesized compounds were found to possess significant antitumor activity. Also, from cytotoxicity and DNA interaction studies, these compounds can also be used for the prevention and treatment of cancer. Gel electrophoresis assay was used to investigate the damage to double stranded super coiled plasmid pBR322 DNA by the synthesized compounds and compounds **1** and **7** were found to cause the maximum damage. All the synthesized compounds exhibit strong antileishmanial activity that was even higher than that of *Amphotericin B*, with significant cytotoxicity. This study, therefore, demonstrated the potential use of these compounds as source of novel agents for the treatment of *leishmaniasis*.

1. Introduction

The chemistry of organotin compounds is gaining attention on account of their interesting structural features, schizonticidal, antimalarial, fungicidal activities and their potential as agricultural biocides [1]. Organotin(IV) compounds of carboxylic acids are being extensively studied with special reference to their methods of synthesis, structural elucidation, and biological activity [2,3]. Encouraged by the initial success of platinum chemotherapeutic metallopharmaceuticals, concentration was first shifted to non-platinum chemotherapeutics starting from the basic *cis*-platin framework, with the aim to optimize the competence of such drugs and to avoid serious side-effects caused by platinum chemotherapeutics. Among these, organotins have appeared as biologically active metallopharmaceuticals [4]. It has well been established that organotin(IV) compounds are very important in cancer chemotherapy because of their apoptosis inducing character, while during the last few years it is noticeable that organotin compounds occupy an important place in cancer chemotherapy reports [5]. Recently, Blower described thirty interesting inorganic pharmaceuticals, four of which are tin compounds [6]. The organotin compounds have also received considerable attention as antiproliferative, antitumor and anticancer drugs. The activity is due to dissociated organotin(IV) moieties. The biological activity usually associates with the nature of organic ligand, since the organic ligand assists the transportation of the complexes across the cell membrane [5,7–9].

The biological activity of organotin compounds is basically determined by the number and nature of the organic groups bound

* Corresponding author.
E-mail addresses: m.siraj09@yahoo.com, msiraj09@gmail.com (M. Sirajuddin), drsa54@yahoo.com (S. Ali).

http://dx.doi.org/10.1016/j.ejmech.2014.07.028
0223-5234/

to the central tin atom. The $[R_3Sn(IV)]^+$ and $[Ar_3Sn(IV)]^+$ derivatives exert powerful toxic action on the central nervous system. Within the series of $[R_3Sn(IV)]^+$ compounds, the lower homologues (Me, Et) are the most toxic when administrated orally, and the toxicity reduces progressively from propyl to octyl, the latter not being toxic at all [10]. The presence of easily hydrolysable groups (easily dissociable chelating ligands) producing intermediates such as $R_nSn^{(4-n)+}$ ($n = 2$ or 3) moieties, which may bind with DNA or high-affinity site of ATPase (histidine only), the low-affinity site of ATPase, and haemoglobins (histidine and cystine), play an important role in the determination of biological activity of the organotin compounds. Therefore, substantial attempts have been made to characterize model organotin compounds of ligands having hetero donor atoms (O, N and S), and simultaneously several studies have been focused on structure–activity correlations during the last two decades [11].

Keeping in view their biological applications, we are reporting a series of 14 new organotin(IV) carboxylates of N-[(2-methoxyphenyl)]-4-oxo-4-[oxy]butanamide. These compounds were characterized successfully by elemental analysis, FT-IR, NMR (^1H, ^{13}C, ^{119}Sn) mass and single crystal analysis. They were screened for biological applications including interaction with SS-DNA, antimicrobial, antitumor, antileishmanial and cytotoxic activities.

2. Experimental section

2.1. Materials and methods

Reagents Me_3SnCl, Bu_3SnCl, Ph_3SnCl, Cy_3SnCl, Me_2SnCl_2, Bu_2SnCl_2, *tert*-Bu_2SnCl_2, Ph_2SnCl_2, *n*-Oct_2SnO, *o*-anisidine, succinic anhydride were obtained from Aldrich (USA) and were used without further purification. All the solvents purchased from E. Merck (Germany) were dried before use according to literature procedures [12]. Dibenzyltin dichloride (Bz_2SnCl_2) and tribenzyltin chloride (Bz_3SnCl) were prepared according to the reported method [13]. Sodium salt of Salmon fish sperm DNA (SS-DNA) (Arcos) was used as received. The melting points were determined in a capillary tube using a Gallenkamp (UK) electrothermal melting point apparatus. IR spectra in the range of 4000–100 cm^{-1} were obtained on a Thermo Nicolet-6700 FT-IR Spectrophotometer. Elemental analysis was done using a CE-440 Elemental Analyzer (Exeter Analytical, Inc) and the experimentally found values are given in parenthesis in experimental part. ^1H, ^{13}C and ^{119}Sn NMR were recorded on a 400 MHz JEOL ECS instrument, using DMSO as an internal reference [^1H (DMSO-d6) = 2.50 and ^{13}C (DMSO-d6) = 39.5 ppm]. Tetramethylsilane (for ^1H and ^{13}C NMR) and Me_4Sn (for ^{119}Sn NMR) were used as external standards. For ^{119}Sn NMR the measurement was recorded at a working frequency of 37.29 MHz and the chemical shift was referenced to Me_4Sn as an external standard. Chemical shifts are given in ppm and coupling constants (J) values are given in Hz. The multiplicities of signals in ^1H NMR are given with chemical shifts; (s = singlet, d = doublet, t = triplet, q = quartet, m = multiplet). The absorption spectra were measured on a Shimadzu 1800 UV–visible Spectrophotometer. X-ray data for **HL** and complex **6** were collected at room temperature while complexes **1** and **2** at 150 (2) K on a Bruker Apex II CCD diffractometer. Complex **3** was collected at 190 (2) K on Agilent Super Nova (Dual, Cu at zero, Eos) diffractometer. Details are given in Table 2. All the non-hydrogen atoms were refined using anisotropic atomic displacement parameters, and hydrogen atoms bonded to carbon were inserted at calculated positions using a riding model. Hydrogen atoms bonded to O or N were located from difference maps and their coordinates refined. SHELXS-97 [14] was used to solve and SHELX2012 [15] to refine the structures. The mass spectra were recorded on a Thermo Scientific executive (orbitrap) utilizing an Advion TriVersa ™NanoMate sample introduction system. The *m/z* values were evaluated assuming that H = 1, C = 12, N = 14, O = 16, Cl = 35, and Sn = 120.

2.2. Synthesis

2.2.1. Synthesis of ligand: N-[(2-methoxyphenyl)]-4-oxo-4-[oxy] butanamide (*HL*)

Stoichiometric amounts of *o*-anisidine (2-methoxyaniline) and succinic anhydride were dissolved separately in glacial acetic acid. The *o*-anisidine solution was added slowly to the solution of succinic anhydride and precipitate appeared [16] (Scheme 1). The precipitates were filtered, washed thoroughly with distilled water (to remove the unreacted succinic acid and succinic anhydride) and HCl (to remove unreacted aniline) and air dried. Prism-like white single crystals of the **HL** used in X-ray diffraction studies were grown in an acetone solution by slow evaporation of solvent at room temperature.

Yield: 90%: M.p. 141–142 °C: Mol. Wt.: 223.23: Anal. Calc. for $C_{11}H_{13}NO_4$: C, 59.2 (59.1); H, 5.9 (5.8); N, 6.3 (6.6): **IR** (4000–100 cm^{-1}): 3200 ν (OH); 3368 ν (NH); 1708 ν (amide C=O); 1595 ν (COOasym); 1289 ν (COOsym); 306 ($\Delta\nu$); **^{1}H NMR** (DMSO-d_6, 400 MHz) δ (ppm): 12.12 (s, 1H; OH); 2.67 (*t*, 2H, H2, $^3J[^1H, ^1H] = 6.6$ Hz); 2.53 (*t*, 2H, H3, $^3J[^1H, ^1H] = 6.6$ Hz); 9.12 (s, 1H NH); 7.98 (d, 1H, H6, $^3J[^1H, ^1H] = 7.8$ Hz); 6.91 (dd, 1H, H8, $^4J[^1H, ^1H] = 2.8$ Hz); 7.08 (m, 2H, H7 and H9); 3.82 (s, 3H, H11): **^{13}C NMR** (DMSO-d_6, 100 MHz) δ (ppm): 174.4 (C1); 31.4 (C2); 29.4 (C3); 170.7 (C4); 127.9 (C5); 122.1 (C6); 120.6 (C7); 124.5 (C8); 111.5 (C9); 149.8 (C10); 56.1 (C11); **ESI-MS**, *m/z* (%): $[C_{11}H_{13}NO_4]^+$ 223 (30.1); $[C_{11}H_{11}NO_3]^+$ 205 (11.3); $[C_7H_9NO]^+$ 123 (100); $[C_7H_8O]^+$ 108 (65.8); $[C_6H_6N]^+$ 92 (5.5); $[C_5H_5]^+$ 65 (7.1); $[C_3H_3O]^+$ 55 (10.4).

2.2.2. Synthesis of sodium salt of ligand: sodium N-[(2-methoxyphenyl)]-4-oxo-4-[oxy]butanamide (*NaL*)

An aqueous solution of sodium hydrogen carbonate ($NaHCO_3$) was added to a suspended solution of **HL** in distilled water. The mixture was stirred at room temperature to get a clear solution which was then rotary evaporated to get the desired sodium salt of the ligand. The chemical reaction is shown in Scheme 1.

2.2.3. Synthesis of organotin(IV) complexes R_3SnL with R = Me (*1*), Bu (*2*), Ph (*3*), and $[R_2SnL_2]$ with R = Me (*4*), Bu (*5*)

Organotin(IV) carboxylates were synthesized by refluxing a mixture of R_3SnCl (5 mmol) or R_2SnCl_2 (2.5 mmol) and the sodium salt of ligand **NaL** (5 mmol) in dry toluene for 8 h (Scheme 2). The refluxed solution was kept overnight at room temperature. The NaCl precipitate was removed by filtration and the solvent was removed under reduced pressure. The product was purified by recrystallization from chloroform at room temperature. The numbering of **HL** and alkyl groups attached to Sn is given in Scheme 3.

2.2.4. N-[(2-methoxyphenyl)]-4-oxo-4-[(trimethylstannyl)oxy] butanamide (*1*)

Yield: 83%: M.p. 115–117 °C: Mol. Wt.: 386.03: Anal. Calc. for $C_{14}H_{21}NO_4Sn$: C, 43.6 (43.2); H, 5.5 (5.2); N, 3.6 (3.7): **IR** (4000–100 cm^{-1}): 3418 ν (NH); 1689 ν (amide C=O); 1557 ν (COOasym); 1394 ν (COOsym); 146 ($\Delta\nu$); 546 ν (Sn–C); 455 ν (Sn–O): **^{1}H NMR** (DMSO-d_6, 400 MHz) δ (ppm): 2.55 (*t*, 2H, H2, $^3J[^1H, ^1H] = 6.8$ Hz); 2.36 (*t*, 2H, H3, $^3J[^1H, ^1H] = 6.8$ Hz); 9.04 (s, 1H NH); 8.02 (d, 1H, H6, $^3J[^1H, ^1H] = 7.8$ Hz); 6.90 (dd, 1H, H8, $^4J[^1H, ^1H] = 2.8$ Hz); 7.03 (m, 2H, H7 and H9); 3.81 (s, 3H, H11); 0.38 (s, 3H, Hα, $^2J[^{119/117}Sn–^1H\alpha] = 70, 68$ Hz): **^{13}C NMR** (DMSO-d_6, 100 MHz) δ (ppm): 176.5 (C1); 33.1 (C2); 31.7 (C3); 171.4 (C4); 128.1 (C5); 121.7 (C6); 120.6 (C7); 124.2 (C8); 111.4 (C9); 149.6 (C10); 56.0 (C11); 0.7 (Cα, $^1J[^{119/}$

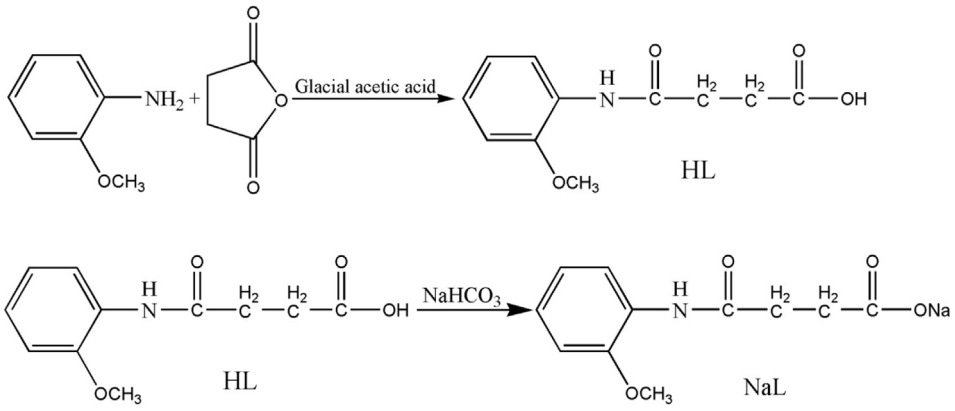

Scheme 1. Structural representation of the ligand (HL) and its sodium salt (NaL).

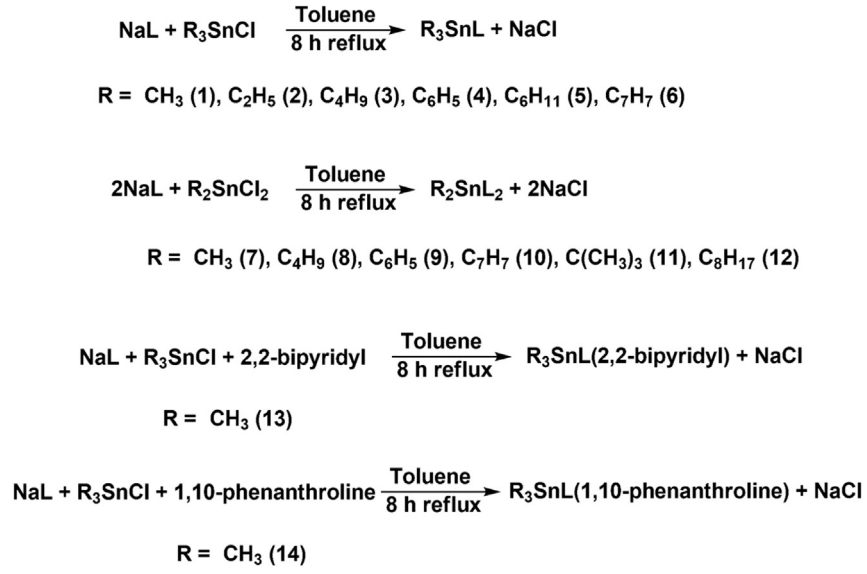

Scheme 2. General representation for synthesis of organotin(IV) compounds.

$^{117}Sn-^{13}C\alpha$ = 524, 500 Hz]): **^{119}Sn NMR** (DMSO-d_6, 400 MHz) δ (ppm): −10.2: **ESI-MS**, *m/z* (%): $[C_{14}H_{21}NO_4SnNa]^+$, *m/z* = 410 (38); $[C_{14}H_{21}NO_4Sn]^+$, *m/z* = 387 (4); $[C_{11}H_{12}O_4N]^+$, *m/z* = 222 (7); $[C_{10}H_{12}NO_2]^+$, *m/z* = 178 (16); $[C_3H_9Sn]^+$, *m/z* = 165 (100); $[C_2H_6Sn]^+$,

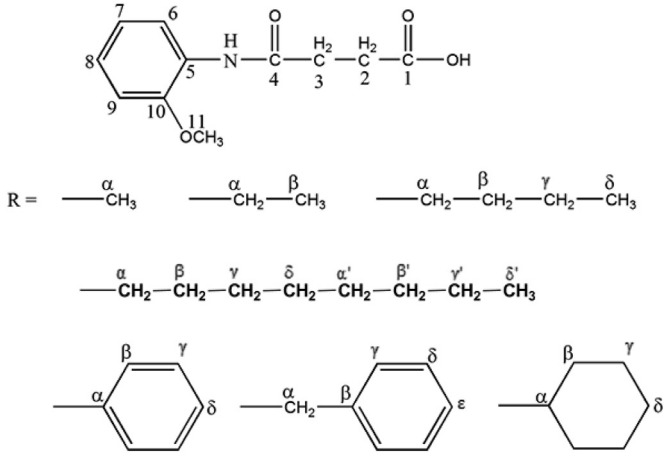

Scheme 3. Numbering pattern of HL and organic moiety attached to Sn atom.

m/z = 150 (25); $[CH_3Sn]^+$, *m/z* = 135 (23); $[Sn]^+$, *m/z* = 120 (32); $[C_{13}H_{18}NO_4Sn]^+$, *m/z* = 372 (41); $[C_{12}H_{18}NO_2Sn]^+$, *m/z* = 328 (3); $[C_{11}H_{15}NO_2Sn]^+$, *m/z* = 313 (17); $[C_{10}H_{12}NO_2Sn]^+$, *m/z* = 298 (20).

*2.2.5. N-[(2-methoxyphenyl)]-4-oxo-4-[(triethylstannyl)oxy] butanamide (**2**)*

Yield: 75%: M.p. 105–106 °C: Mol. Wt.: 428.11: Anal. Calc. for $C_{17}H_{27}NO_4Sn$: C, 47.7 (47.6); H, 6.4 (6.9); N, 3.3 (3.5): **IR** (4000–100 cm^{-1}): 3434 ν (NH); 1695 ν (amide C=O); 1562 ν (COOasym); 1392 ν (COOsym); 170 ($\Delta\nu$); 521 ν (Sn–C); 481 ν (Sn–O): **^{1}H NMR** (DMSO-d_6, 400 MHz) δ (ppm): 2.58 (*t*, 2H, H2, ^3J[^{1}H, ^{1}H] = 6.4 Hz); 2.41 (*t*, 2H, H3, ^3J[^{1}H, ^{1}H] = 6.4 Hz); 9.04 (s, 1H NH); 8.00 (d, 1H, H6, ^3J[^{1}H, ^{1}H] = 7.8 Hz); 6.90 (dd, 1H, H8, ^4J[^{1}H, ^{1}H] = 2.4 Hz); 7.06 (m, 2H, H7 and H9); 3.81 (s, 3H, H11); 1.08 (*q*, 2H, Hα); 1.23 (*t*, 3H, Hβ, ^3J[^{1}H, ^{1}H] = 8.0 Hz): **^{13}C NMR** (DMSO-d_6, 100 MHz) δ (ppm): 176.7 (C1); 33.2 (C2); 31.6 (C3); 171.3 (C4); 128.1 (C5); 121.8 (C6); 120.6 (C7); 124.2 (C8); 111.3 (C9); 149.6 (C10); 56.0 (C11); 11.4 (Cα); 10.7 (Cβ, ^2J[^{119}Sn–^{13}Cβ] = 32.3 Hz): **^{119}Sn NMR** (DMSO-d_6, 400 MHz) δ (ppm): −18.8: **ESI-MS**, *m/z* (%): $[C_{17}H_{27}NO_4SnNa]^+$, *m/z* = 452 (42); $[C_{17}H_{27}NO_4Sn]^+$, *m/z* = 429 (2); $[C_{11}H_{12}O_4N]^+$, *m/z* = 222 (24); $[C_{10}H_{12}NO_2]^+$, *m/z* = 178 (7); $[C_6H_{15}Sn]^+$, *m/z* = 207 (100); $[C_4H_{10}Sn]^+$, *m/z* = 178 (7); $[C_2H_5Sn]^+$, *m/z* = 149 (5); $[Sn]^+$, *m/z* = 120 (8); $[C_{15}H_{22}NO_4Sn]^+$, *m/z* = 400

(98); $[C_{14}H_{22}NO_2Sn]^+$, m/z = 356 (4); $[C_{12}H_{17}NO_2Sn]^+$, m/z = 327 (2); $[C_{10}H_{12}NO_2Sn]^+$, m/z = 298 (15).

2.2.6. N-[(2-methoxyphenyl)]-4-oxo-4-[(tributylstannyl)oxy] butanamide (**3**)

Yield: 76%: M.p. 52–54 °C: $C_{23}H_{39}NO_4Sn$ Mol. Wt.: 512.27: Anal. Calc. for $C_{17}H_{27}NO_4Sn$: C, 53.9 (53.8); H, 7.7 (7.4); N, 2.7 (2.9): **IR** (4000–100 cm^{-1}): 3426 ν (NH); 1694 ν (amide C=O); 1552 ν (COOasym); 1372 ν (COOsym); 180 ($\Delta\nu$); 569 ν (Sn–C); 455 ν (Sn–O): **^{1}H NMR** (DMSO-d_6, 400 MHz) δ (ppm): 2.55 (*t*, 2H, H2, ^3J[^{1}H, ^{1}H] = 6.8 Hz); 2.38 (*t*, 2H, H3, ^3J[^{1}H, ^{1}H] = 6.8 Hz); 9.00 (s, 1H NH); 8.02 (d, 1H, H6, ^3J[^{1}H, ^{1}H] = 7.8 Hz); 6.88 (dd, 1H, H8, ^4J[^{1}H, ^{1}H] = 2.4 Hz); 7.02 (m, 2H, H7 and H9); 3.81 (s, 3H, H11); 1.07 (*t*, 3H, Hα, ^3J[^{1}H, ^{1}H] = 8.0 Hz); 1.56 (m, 2H, Hβ); 1.33 (m, 2H, Hγ); 0.87 (*t*, 3H, Hδ, ^3J[^{1}H, ^{1}H] = 6.8 Hz): **^{13}C NMR** (DMSO-d_6, 100 MHz) δ (ppm): 176.4 (C1); 33.2 (C2); 31.7 (C3); 171.3 (C4); 128.2 (C5); 121.6 (C6); 120.5 (C7); 124.1 (C8); 111.3 (C9); 149.5 (C10); 56.0 (C11); 19.1 (Cα); 28.1 (Cβ, ^2J[^{119}Sn–^{13}Cβ] = 27 Hz) 26.9 (Cγ, ^3J[^{119}Sn–^{13}Cγ] = 75 Hz); 14.1 (Cδ): **^{119}Sn NMR** (DMSO-d_6, 400 MHz) δ (ppm): −17.6. **ESI-MS**, m/z (%): $[C_{23}H_{39}NO_4SnNa]^+$, m/z = 536 (27); $[C_{23}H_{39}NO_4Sn]^+$, m/z = 513 (20); $[C_{11}H_{12}NO_4]^+$, m/z = 222 (8); $[C_{10}H_{12}NO_2]^+$, m/z = 178 (11); $[C_{12}H_{27}Sn]^+$, m/z = 291 (100); $[C_8H_{18}Sn]^+$, m/z = 234 (26); $[C_4H_9Sn]^+$, m/z = 177 (20); $[Sn]^+$, m/z = 120 (12); $[C_{19}H_{30}NO_4Sn]^+$, m/z = 456 (22); $[C_{18}H_{30}NO_2Sn]^+$, m/z = 412 (7); $[C_{14}H_{21}NO_2Sn]^+$, m/z = 355 (12); $[C_{10}H_{12}NO_2Sn]^+$, m/z = 298 (3).

2.2.7. N-[(2-methoxyphenyl)]-4-oxo-4-[(triphenylstannyl)oxy] butanamide (**4**)

Yield: 87%: M.p. 102–103 °C: Mol. Wt.: 572.24: Anal. Calc. for $C_{29}H_{27}NO_4Sn$: C, 60.9 (60.5); H, 4.8 (4.2); N, 2.5 (2.8): **IR** (4000–100 cm^{-1}): 3425 ν (NH); 1645 ν (amide C=O); 1545 ν (COOasym); 1382 ν (COOsym); 163 ($\Delta\nu$); 267 ν (Sn–C); 444 ν (Sn–O): **^{1}H NMR** (DMSO-d_6, 400 MHz) δ (ppm): 2.51 (*t*, 2H, H2, ^3J[^{1}H, ^{1}H] = 6.4 Hz); 2.39 (*t*, 2H, H3, ^3J[^{1}H, ^{1}H] = 6.4 Hz); 9.02 (s, 1H NH); 8.00 (d, 1H, H6, ^3J[^{1}H, ^{1}H] = 7.8 Hz); 6.91 (dd, 1H, H8, ^4J[^{1}H, ^{1}H] = 2.4 Hz); 7.05 (m, 2H, H7 and H9); 3.77 (s, 3H, H11); 7.91 (m, 15 H, Sn–Ph): **^{13}C NMR** (DMSO-d_6, 100 MHz) δ (ppm): 176.3 (C1); 32.9 (C2); 31.6 (C3); 171.2 (C4); 128.1 (C5); 121.8 (C6); 120.6 (C7); 124.3 (C8); 111.4 (C9); 149.6 (C10); 56.0 (C11); 143.5 (C_α); 136.7 (C_β, ^2J[^{119}Sn–$^{13}C_\beta$] = 46 Hz); 128.6 (C_γ, ^3J[^{119}Sn–$^{13}C_\delta$] = 63 Hz); 129.4 (C_δ): **^{119}Sn NMR** (DMSO-d_6, 400 MHz) δ (ppm): −246.9: **ESI-MS**, m/z (%): $[C_{29}H_{27}NO_4SnNa]^+$, m/z = 596 (15); $[C_{29}H_{27}NO_4Sn]^+$, m/z = 573 (13); $[C_{11}H_{12}NO_4]^+$, m/z = 222 (9); $[C_{10}H_{12}NO_2]^+$, m/z = 178 (10); $[C_{18}H_{15}Sn]^+$, m/z = 351 (100); $[C_{12}H_{10}Sn]^+$, m/z = 274 (25); $[C_4H_9Sn]^+$, m/z = 197 (23); $[Sn]^+$, m/z = 120 (10); $[C_{23}H_{22}NO_4Sn]^+$, m/z = 496 (12); $[C_{22}H_{22}NO_2Sn]^+$, m/z = 452 (24); $[C_{16}H_{17}NO_2Sn]^+$, m/z = 375 (21); $[C_{10}H_{12}NO_2Sn]^+$, m/z = 298 (35).

2.2.8. N-[(2-methoxyphenyl)]-4-oxo-4-[(tricyclohexylstannyl)oxy] butanamide (**5**)

Yield: 84%: M.p. 85–87 °C: Mol. Wt.: 590.38: Anal. Calc. $C_{29}H_{45}NO_4Sn$: C, 59.0 (58.7); H, 7.7 (7.5); N, 2.4 (2.6): **IR** (4000–100 cm^{-1}): 3426 ν (NH); 1694 ν (amide C=O); 1577 ν (COOasym); 1393 ν (COOsym); 184 ($\Delta\nu$); 569 ν (Sn–C); 455 ν (Sn–O): **^{1}H NMR** (DMSO-d_6, 400 MHz) δ (ppm): 2.58 (*t*, 2H, H2, ^3J[^{1}H, ^{1}H] = 6.4); 2.46 (*t*, 2H, H3, ^3J[^{1}H, ^{1}H] = 6.4); 9.05 (s, 1H NH); 8.04 (d, 1H, H6, ^3J[^{1}H, ^{1}H] = 7.8 Hz); 6.88 (dd, 1H, H8, ^4J[^{1}H, ^{1}H] = 2.4 Hz); 7.01 (m, 2H, H7 and, H9); 3.82 (s, 3H, H11); 1.19 (m, 1H, Hα); 1.84 (m, 2H, Hβ); 1.62 (m, 2H, Hγ); 1.58 (m, 2H, Hδ): **^{13}C NMR** (DMSO-d_6, 100 MHz) δ (ppm): 176.8 (C1); 33.2 (C2); 31.4 (C3); 171.2 (C4); 128.2 (C5); 121.6 (C6); 120.5 (C7); 124.1 (C8); 111.3 (C9); 149.5 (C10); 56.0 (C11); 27.1 (Cα, ^1J[^{119}Sn–^{13}Cα] = 512 Hz); 29.2 (Cβ, ^2J[^{119}Sn–^{13}Cβ] = 72 Hz) 36.1 (Cγ) 30.9 (Cδ, ^4J[^{119}Sn–^{13}Cγ] = 47 Hz): **^{119}Sn NMR** (DMSO-d_6, 400 MHz) δ (ppm): −250.4: **ESI-MS**, m/z (%): $[C_{29}H_{45}NO_4SnNa]^+$, m/z = 614 (22); $[C_{29}H_{45}NO_4Sn]^+$, m/z = 591 (15); $[C_{11}H_{12}NO_4]^+$, m/z = 222 (27); $[C_{10}H_{12}NO_2]^+$, m/z = 178 (18); $[C_{18}H_{33}Sn]^+$, m/z = 369 (100); $[C_{12}H_{22}Sn]^+$, m/z = 287 (15); $[C_6H_{11}Sn]^+$, m/z = 197 (29); $[Sn]^+$, m/z = 120 (15); $[C_{23}H_{34}NO_4Sn]^+$, m/z = 508 (23); $[C_{22}H_{34}NO_2Sn]^+$, m/z = 464 (21); $[C_{16}H_{23}NO_2Sn]^+$, m/z = 381 (14); $[C_{10}H_{12}NO_2Sn]^+$, m/z = 298 (18).

2.2.9. N-[(2-methoxyphenyl)]-4-oxo-4-[(tribenzylstannyl)oxy] butanamide (**6**)

Yield: 81%: M.p. 112–114 °C: Anal. Calc. $C_{32}H_{33}NO_4Sn$: Mol. Wt.: 614.3: C, 62.6; H, 5.4 (5.3); N, 2.3 (2.3): **IR** (4000–100 cm^{-1}): 3426 ν (NH); 1685 ν (amide C=O); 1559 ν (COOasym); 1357 ν (COOsym); 202 ($\Delta\nu$); 542 ν (Sn–C); 447 ν (Sn–O): **^{1}H NMR** (DMSO-d_6, 400 MHz) δ (ppm): 2.46 (*t*, 2H, H2, ^3J[^{1}H, ^{1}H] = 6.8 Hz); 2.31 (*t*, 2H, H3, ^3J[^{1}H, ^{1}H] = 6.8 Hz); 8.96 (s, 1H NH); 7.94 (d, 1H, H6, ^3J[^{1}H, ^{1}H] = 8.0 Hz); 6.97 (dd, 1H, H8, ^4J[^{1}H, ^{1}H] = 3.6 Hz); 7.44 (m, 2H, H7 and H9); 3.73 (s, 3H, H11); 2.05 (s, 2H, Hα, ^2J[^{119}Sn–^{1}H] = 61); 7.14 (d, 1H, Hγ, ^3J[^{1}H, ^{1}H] = 7.6 Hz); 7.21 (*t*, 2H, Hδ, ^3J[^{1}H, ^{1}H] = 8.0 Hz); 6.84 (*t*, 1H, Hε, ^3J[^{1}H, ^{1}H] = 8.0 Hz): **^{13}C NMR** (DMSO-d_6, 100 MHz) δ (ppm): 176.3 (C1); 31.5 (C2); 30.5 (C3); 171.2 (C4); 128.2 (C5); 121.9 (C6); 120.7 (C7); 124.3 (C8); 111.5 (C9); 149.7 (C10); 56.1 (C11); 21.6 (Cα, ^1J[^{119}Sn–^{13}Cα] = 483 Hz); 143.7 (Cβ, ^2J[^{119}Sn–^{13}Cβ] = 72 Hz), 128.7 (Cγ, ^3J[^{119}Sn–^{13}Cγ] = 62 Hz), 136.8 (Cδ, ^4J[^{119}Sn–^{13}Cδ] = 46 Hz), 125.9 (Cε): **^{119}Sn NMR** (DMSO-d_6, 400 MHz) δ (ppm): −256.9: **ESI-MS**, m/z (%): $[C_{32}H_{33}NO_4SnNa]^+$, m/z = 638 (60); $[C_{32}H_{33}NO_4Sn]^+$, m/z = 615 (15); $[C_{32}H_{33}NO_4Sn]^+$, m/z = 616 (98); $[C_{11}H_{12}NO_4]^+$, m/z = 222 (16); $[C_9H_{12}NO_2]^+$, m/z = 178 (23); $[C_{32}H_{32}Sn]^+$, m/z = 393 (100); $[C_{12}H_{22}Sn]^+$, m/z = 302 (23); $[C_6H_{11}Sn]^+$, m/z = 211 (9); $[Sn]^+$, m/z = 120 (5); $[C_{25}H_{26}NO_4Sn]^+$, m/z = 524 (21); $[C_{25}H_{26}NO_2Sn]^+$, m/z = 480 (26); $[C_{16}H_{17}NO_2Sn]^+$, m/z = 389 (3); $[C_{10}H_{11}N_2O_4Sn]^+$, m/z = 343 (21).

2.2.10. Dimethylstannanediyl bis(4-(2-methoxyphenylamino)-4-oxobutanoate) (**7**)

Yield: 870%: M.p. 120–122 °C: Mol. Wt.: 593.21: Anal. Calc. for $C_{24}H_{30}N_2O_8Sn$: C, 48.6 (62.6); H, 5.1 (5.3); N, 4.7 (4.4): **IR** (4000–100 cm^{-1}): 3253 ν (NH); 1664 ν (amide C=O); 1526 ν (COOasym); 1386 ν (COOsym); 140 ($\Delta\nu$); 577 ν (Sn–C); 450 ν (Sn–O): **^{1}H NMR** (DMSO-d_6, 400 MHz) δ (ppm): 2.66 (*t*, 2H, H2, ^3J[^{1}H, ^{1}H] = 6.6); 2.50 (*t*, 2H, H3, ^3J[^{1}H, ^{1}H] = 6.6); 9.11 (s, 1H NH); 8.0 (d, ^3J[^{1}H, ^{1}H] = 7.8 Hz, 1H, H6); 6.91 (dd, 1H, H8, ^4J[^{1}H, ^{1}H] = 2.4 Hz); 7.07 (m, 2H, H7 and H9); 3.82 (s, 3H, H11); 0.76 (s, 3H, Hα) [$^{119/117}$Sn–^{1}H] = 102, 100 Hz): **^{13}C NMR** (DMSO-d_6, 100 MHz) δ (ppm): 178.8 (C1); 32.1 (C2); 30.1 (C3); 170.8 (C4); 128.0 (C5); 121.9 (C6); 120.6 (C7); 124.4 (C8); 111.4 (C9); 149.7 (C10); 56.0 (C11); 12.7 (Cα): **^{119}Sn NMR** (DMSO-d_6, 400 MHz) δ (ppm): −281.7: **ESI-MS**, m/z (%): $[C_{24}H_{30}N_2O_8SnNa]^+$, m/z = 617 (34); $[C_{24}H_{30}N_2O_8Sn]^+$, m/z = 594 (20); $[C_{23}H_{27}N_2O_8Sn]^+$, m/z = 579 (18); $[C_{12}H_{15}NO_4Sn]^+$, m/z = 357 (19); $[C_{11}H_{12}NO_4Sn]^+$, m/z = 342 (20); $[C_{11}H_{12}NO_4]^+$, m/z = 222 (11); $[C_9H_{12}NO_2]^+$, m/z = 178 (13); $[C_2H_6Sn]^+$, m/z = 150 (10); $[CH_3Sn]^+$, m/z = 135 (14); $[Sn]^+$, m/z = 120 (4); $[C_{13}H_{18}NO_4Sn]^+$, m/z = 372 (100); $[C_{12}H_{18}NO_2Sn]^+$, m/z = 328 (21); $[C_{11}H_{15}NO_2Sn]^+$, m/z = 313 (27); $[C_{10}H_{12}NO_2Sn]^+$, m/z = 298 (25); $[C_{22}H_{27}N_2O_6Sn]^+$, m/z = 535 (12).

2.2.11. Dibutylstannanediyl bis(4-(2-methoxyphenylamino)-4-oxobutanoate) (**8**)

Yield: 80%: M.p. 115–117 °C: Mol. Wt.: 677.37: Anal. Calc. for $C_{30}H_{42}N_2O_8Sn$: C, 53.2 (53.5); H, 6.3 (6.6); N, 4.1 (4.5): **IR** (4000–100 cm^{-1}): 3312 ν (NH); 1698 ν (amide C=O); 1525 ν (COOasym); 1391 ν (COOsym); 134 ($\Delta\nu$); 571 ν (Sn–C); 477 ν (Sn–O): **^{1}H NMR** (DMSO-d_6, 400 MHz) δ (ppm): 2.65 (*t*, 2H, H2, ^3J[^{1}H, ^{1}H] = 6.4); 2.52 (*t*, 2H, H3, ^3J[^{1}H, ^{1}H] = 6.4); 9.10 (s, 1H NH); 8.04 (d, ^3J[^{1}H, ^{1}H] = 7.5 Hz, 1H, H6); 6.89 (dd, 1H, H8, ^4J[^{1}H, ^{1}H] = 2.4 Hz); 7.06 (m, 2H, H7 and H9); 3.82 (s, 3H, H11); 1.20 (*t*, 3H, Hα, ^3J[^{1}H, ^{1}H) = 7.2 Hz); 1.46 (m, 2H, Hβ); 1.35 (m, 2H, Hγ); 0.77 (*t*, 3H, Hδ, ^3J[^{1}H, ^{1}H] = 7.2 Hz): **^{13}C NMR** (DMSO-d_6, 100 MHz) δ (ppm): 179.5 (C1); 32.2

(C2); 29.9 (C3); 170.8 (C4); 128.0 (C5); 121.8 (C6); 120.5 (C7); 124.3 (C8); 111.3 (C9); 149.6 (C10); 56.0 (C11): 21.4 (Cα); 28.1 (Cβ, ^2J [^{119}Sn–^{13}Cβ = 27 Hz); 26.2 (Cγ, ^3J[^{119}Sn–^{13}Cγ] = 75 Hz) 14.1 (Cδ): **^{119}Sn NMR** (DMSO-d_6, 400 MHz) δ (ppm): −296.7: **ESI-MS**, *m/z* (%): $[C_30H_{42}N_2O_8SnNa]^+$, *m/z* = 701 (54); $[C_{30}H_{42}N_2O_8Sn]^+$, *m/z* = 678 (12); $[C_{26}H_{33}N_2O_8Sn]^+$, *m/z* = 621 (7); $[C_{15}H_{21}NO_4Sn]^+$, *m/z* = 399 (8); $[C_{11}H_{12}NO_4Sn]^+$, *m/z* = 342 (4); $[C_{11}H_{12}NO_4]^+$, *m/z* = 222 (11); $[C_{10}H_{12}NO_2]^+$, *m/z* = 178 (12); $[C_8H_{18}Sn]^+$, *m/z* = 234 (7); $[C_4H_9Sn]^+$, *m/z* = 177 (100); $[Sn]^+$, *m/z* = 120 (12); $[C_{19}H_{30}NO_4Sn]^+$, *m/z* = 456 (24); $[C_{18}H_{30}NO_2Sn]^+$, *m/z* = 412 (6); $[C_{14}H_{21}NO_2Sn]^+$, *m/z* = 355 (5); $[C_{10}H_{12}NO_2Sn]^+$, *m/z* = 298 (5); $[C_{25}H_{33}N_2O_6Sn]^+$, *m/z* = 577 (4).

2.2.12. Diphenylstannanediyl bis(4-(2-methoxyphenylamino)-4-oxobutanoate) (**9**)

Yield: 78%: M.p. 121–123 °C: Mol. Wt.: 717.35: Anal. Calc. for $C_{34}H_{34}N_2O_8Sn$: C, 56.9 (56.2); H, 4.8 (4.4); N, 3.9 (3.6): **IR** (4000–100 cm^{-1}): 3277 ν (NH); 1646 ν (amide C=O); 1541 ν (COOasym); 1381 ν (COOsym); 160 (Δν); 280 ν (Sn–C); 451 ν (Sn–O): **^{1}H NMR** (DMSO-d_6, 400 MHz) δ (ppm): 2.50 (*t*, 2H, H2, ^3J [^{1}H, ^{1}H] = 6.6); 2.36 (*t*, 2H, H3, ^3J[^{1}H, ^{1}H] = 6.6); 9.02 (s, 1H NH); 8.00 (d, ^3J[^{1}H, ^{1}H] = 7.5 Hz, 1H, H6); 6.91 (dd, 1H, H8, ^4J[^{1}H, ^{1}H] = 2.2); 7.07 (m, 2H, H7 and H9); 3.77 (s, 3H, H11); 7.90 (m, 10 H, Sn–Ph): **^{13}C NMR** (DMSO-d_6, 100 MHz) δ (ppm): 176.3 (C1); 32.9 (C2); 31.7 (C3); 171.2 (C4); 128.0 (C5); 121.9 (C6); 120.6 (C7); 124.3 (C8); 111.4 (C9); 149.6 (C10); 56.0 (C11): 143.6 (Cα), 136.7 (Cβ, ^2J [^{119}Sn–^{13}Cβ] = 45.8 Hz), 128.6 (Cγ, ^3J[$^{119/117}$Sn–^{13}Cγ] = 74, 68), 129.4 (Cδ, ^4J[^{119}Sn–^{13}Cδ] = 63 Hz]): **^{119}Sn NMR** (DMSO-d_6, 400 MHz) δ (ppm): −256.7: **ESI-MS**, *m/z* (%): $[C_{34}H_{34}N_2O_8SnNa]^+$, *m/z* = 741 (20); $[C_{34}H_{34}N_2O_8Sn]^+$, *m/z* = 718 (12); $[C_{28}H_{29}N_2O_8Sn]^+$, *m/z* = 641 (4); $[C_{17}H_{17}NO_4Sn]^+$, *m/z* = 419 (10); $[C_{11}H_{12}NO_4Sn]^+$, *m/z* = 342 (11); $[C_{11}H_{12}NO_4]^+$, *m/z* = 222 (10); $[C_{10}H_{12}NO_2]^+$, *m/z* = 178 (12); $[C_{12}H_{10}Sn]^+$, *m/z* = 274 (13); $[C_6H_5Sn]^+$, *m/z* = 197 (100); $[Sn]^+$, *m/z* = 120 (9); $[C_{23}H_{22}NO_4Sn]^+$, *m/z* = 496 (12); $[C_{22}H_{22}NO_2Sn]^+$, *m/z* = 452 (9); $[C_{16}H_{17}NO_2Sn]^+$, *m/z* = 375 (7); $[C_{10}H_{12}NO_2Sn]^+$, *m/z* = 298 (3); $[C_{27}H_{29}N_2O_6Sn]^+$, *m/z* = 597 (19).

2.2.13. Dibenzylstannanediyl bis[4-(2-methoxyphenylamino)-4-oxobutanoate] (**10**)

Yield: 70%: M.p. 131–133 °C: Mol. Wt.: 745.41: Anal. Calc. for $C_{36}H_{38}N_2O_8Sn$: C, 58.0 (58.2); H, 5.1 (4.9); N, 3.8 (3.6): **IR** (4000–100 cm^{-1}): 3299 ν (NH); 1665 ν (amide C=O); 1530 ν (COOasym); 1371 ν (COOsym); 159 (Δν); 538 ν (Sn–C); 444 ν (Sn–O): **^{1}H NMR** (DMSO-d_6, 400 MHz) δ (ppm): 2.71 (*t*, 2H, H2, ^3J [^{1}H, ^{1}H] = 6.8 Hz); 2.60 (*t*, 2H, H3, ^3J[^{1}H, ^{1}H] = 6.8 Hz); 9.01 (s, 1H NH); 8.00 (d, ^3J[^{1}H, ^{1}H] = 7.6 Hz, 1H, H6); 6.91 (dd, 1H, H8, ^4J[^{1}H, ^{1}H] = 1.6 Hz); 7.01 (m, 2H, H7 and H9); 3.83 (s, 3H, H11); 1.18 (s, 2H, Hα); 7.95 (d, 1H, Hγ, ^3J(^{1}H, ^{1}H) = 8.0 Hz); 7.23 (*t*, 2H, Hδ, ^3J[^{1}H, ^{1}H] = 7.8 Hz); 6.80 (*t*, 1H, Hε, ^3J[^{1}H, ^{1}H] = 7.8 Hz): **^{13}C NMR** (DMSO-d_6, 100 MHz) δ (ppm): 172.3 (C1); 32.2 (C2); 31.0 (C3); 169.7 (C4); 127.5 (C5); 121.2 (C6); 120.8 (C7); 123.5 (C8); 110.4 (C9); 148.6 (C10); 55.0 (C11): 21.6 (Cα); 143.5 (Cβ), 127.0 (Cγ), 136.6 (Cδ), 126.8 (Cε): **^{119}Sn NMR** (DMSO-d_6, 400 MHz) δ (ppm): −319.8: **ESI-MS**, *m/z* (%): $[C_{36}H_{38}N_2O_8SnNa]^+$, *m/z* = 769 (9); $[C_{36}H_{38}N_2O_8Sn]^+$, *m/z* = 746 (7); $[C_{29}H_{31}N_2O_8Sn]^+$, *m/z* = 655 (14); $[C_{18}H_{19}NO_4Sn]^+$, *m/z* = 433 (15); $[C_{11}H_{12}NO_6Sn]^+$, *m/z* = 342 (4); $[C_{11}H_{12}NO_4]^+$, *m/z* = 222 (10); $[C_{11}H_{13}NO_4]^+$, *m/z* = 224 (100); $[C_{10}H_{12}NO_2]^+$, *m/z* = 178 (12); $[C_{14}H_{14}Sn]^+$, *m/z* = 302 (17); $[C_7H_7Sn]^+$, *m/z* = 211 (17); $[CH_3Sn]^+$, *m/z* = 135 (45); $[Sn]^+$, *m/z* = 120 (2); $[C_{25}H_{26}NO_4Sn]^+$, *m/z* = 524 (44); $[C_{25}H_{26}NO_2Sn]^+$, *m/z* = 480 (12); $[C_{17}H_{19}NO_2Sn]^+$, *m/z* = 389 (5); $[C_{10}H_{12}NO_2Sn]^+$, *m/z* = 298 (9); $[C_{28}H_{31}N_2O_6Sn]^+$, *m/z* = 611 (5).

2.2.14. Di-tert-butylstannanediyl bis[4-(2-methoxyphenylamino)-4-oxobutanoate] (**11**)

Yield: 85%: M.p. 106–108 °C: Mol. Wt.: 677.37: Anal. Calc. for $C_{30}H_{42}N_2O_8Sn$: C, 53.2 (53.5); H, 6.3 (6.0); N, 4.1 (4.6): **IR** (4000–100 cm^{-1}): 3425 ν (NH); 1687 ν (amide C=O); 1526 ν (COOasym); 1397 ν (COOsym); 129 (Δν); 586 ν (Sn–C); 455 ν (Sn–O): **^{1}H NMR** (DMSO-d_6, 400 MHz) δ (ppm): 2.66 (*t*, 2H, H2, ^3J [^{1}H, ^{1}H] = 6.4); 2.52 (*t*, 2H, H3, ^3J[^{1}H, ^{1}H] = 6.4); 9.10 (s, 1H NH); 7.90 (d, ^3J[^{1}H, ^{1}H] = 8.0 Hz, 1H, H6); 6.85 (dd, 1H, H8, ^4J[^{1}H, ^{1}H] = 2.4); 7.02 (m, 2H, H7 and H9); 3.77 (s, 3H, H11); 1.23 (s, 9H, Hβ, ^3J [^{119}Sn–^{1}Hβ] = 31 Hz): **^{13}C NMR** (DMSO-d_6, 100 MHz) δ (ppm): 180.9 (C1); 32.0 (C2); 29.4 (C3); 170.6 (C4); 128.0 (C5); 122.1 (C6); 120.7 (C7); 124.6 (C8); 111.6 (C9); 149.9 (C10); 56.1 (C11): 30.6 (Cα); 29.9 (Cβ): **^{119}Sn NMR** (DMSO-d_6, 400 MHz) δ (ppm): −215.8: **ESI-MS**, *m/z* (%):$[C_{30}H_{42}N_2O_8SnNa]^+$, *m/z* = 701 (100); $[C_{30}H_{42}N_2O_8Sn]^+$, *m/z* = 678 (20); $[C_{30}H_{43}N_2O_8Sn]^+$, *m/z* = 679 (80); $[C_{26}H_{33}N_2O_8Sn]^+$, *m/z* = 621 (2); $[C_{15}H_{21}NO_4Sn]^+$, *m/z* = 399 (12); $[C_{11}H_{12}NO_4Sn]^+$, *m/z* = 342 (1); $[C_{11}H_{12}NO_4]^+$, *m/z* = 222 (10); $[C_{10}H_{12}NO_2]^+$, *m/z* = 178 (8); $[C_8H_{18}Sn]^+$, *m/z* = 234 (7); $[C_4H_9Sn]^+$, *m/z* = 177 (77); $[C_3H_6Sn]^+$, *m/z* = 162 (12); $[C_2H_3Sn]^+$, *m/z* = 147 (7); $[Sn]^+$, *m/z* = 120 (12); $[C_{19}H_{30}NO_4Sn]^+$, *m/z* = 456 (34); $[C_{18}H_{30}NO_2Sn]^+$, *m/z* = 412 (16); $[C_{14}H_{21}NO_2Sn]^+$, *m/z* = 355 (13); $[C_{10}H_{12}NO_2Sn]^+$, *m/z* = 298 (4); $[C_{25}H_{33}N_2O_6Sn]^+$, *m/z* = 577 (15).

2.2.15. Dioctylstannanediyl bis(4-(2-methoxyphenylamino)-4-oxobutanoate) (**12**)

Yield: 73%: M.p. 81–83 °C: Mol. Wt.: 789.59: Anal. Calc. for $C_{38}H_{58}N_2O_8Sn$: C, 57.8 (57.4); H, 7.4 (7.1); N, 3.5 (3.8): **IR** (4000–100 cm^{-1}): 3322 ν (NH); 1690 ν (amide C=O); 1521 ν (COOasym); 1376 ν (COOsym); 145 (Δν); 575 ν (Sn–C); 474 ν (Sn–O): **^{1}H NMR** (DMSO-d_6, 400 MHz) δ (ppm): 2.65 (*t*, 2H, H2, ^3J [^{1}H, ^{1}H] = 6.4); 2.52 (*t*, 2H, H3, ^3J[^{1}H, ^{1}H] = 6.4 Hz); 9.10 (s, 1H NH); 8.04 (d, ^3J[^{1}H, ^{1}H] = 7.5 Hz, 1H, H6); 6.89 (dd, 1H, H8, ^3J[^{1}H, ^{1}H] = 2.4 Hz); 7.06 (m, 2H, H7 and H9); 3.82 (s, 3H, H11); 1.33 (*t*, 2H, Hα, ^3J[^{1}H, ^{1}H] = 6.8 Hz); 1.40 (bs, 6H, Hβ, γ, δ); 1.50 (bs, 6H, Hα′, β′, γ′); 0.83 (*t*, 3H, Hδ′, ^3J[^{1}H, ^{1}H] = 6.8 Hz): **^{13}C NMR** (DMSO-d_6, 100 MHz) δ (ppm): 172.5 (C1); 32.0 (C2); 30.9 (C3); 169.8 (C4); 128.1 (C5); 121.9 (C6); 119.6 (C7); 124.0 (C8); 110.4 (C9); 148.7 (C10); 55.0 (C11): 24.6 (Cα); 29.5 (Cβ); 34.1 (Cγ); 29.3 (Cδ); 29.2 (Cα′); 31.9 (Cβ′); 22.8 (Cγ′); 13.7 (Cδ′): **^{119}Sn NMR** (DMSO-d_6, 400 MHz) δ (ppm): −298.7: **ESI-MS**, *m/z* (%): $[C_{38}H_{58}N_2O_8SnNa]^+$, *m/z* = 813 (43); $[C_{38}H_{58}N_2O_8Sn]^+$, *m/z* = 790 (26); $[C_{30}H_{41}N_2O_8Sn]^+$, *m/z* = 677 (14); $[C_{19}H_{29}NO_4Sn]^+$, *m/z* = 455 (7); $[C_{11}H_{12}NO_4Sn]^+$, *m/z* = 342 (7); $[C_{11}H_{12}NO_4]^+$, *m/z* = 222 (9); $[C_{11}H_{12}NO_4]^+$, *m/z* = 224 (100); $[C_{10}H_{12}NO_2]^+$, *m/z* = 178 (18); $[C_{16}H_{34}Sn]^+$, *m/z* = 346 (4); $[C_8H_{17}Sn]^+$, *m/z* = 233 (5); $[Sn]^+$, *m/z* = 120 (8); $[C_{27}H_{46}NO_4Sn]^+$, *m/z* = 568 (47); $[C_{26}H_{46}NO_2Sn]^+$, *m/z* = 524 (32); $[C_{18}H_{29}NO_2Sn]^+$, *m/z* = 411 (3); $[C_{10}H_{12}N_2O_4Sn]^+$, *m/z* = 298 (1); $[C_{29}H_{41}N_2O_6Sn]^+$, *m/z* = 633 (2).

2.2.16. (2,2′-Bipyridine) N-[(2-methoxyphenyl)]-4-oxo-4-[(trimethylstannyl)oxy]butanamide (**13**)

Yield: 75%: M.p. 110–112 °C: Mol. Wt.: 542.2: Anal. Calc. for $C_{24}H_{29}N_3O_4Sn$: C, 53.2 (53.5); H, 5.4 (5.3); N, 7.8 (7.9): **IR** (4000–100 cm^{-1}): 3416 ν (NH); 1690 ν (amide C=O); 1522 ν (COOasym); 1392 ν (COOsym); 130 (Δν); 546 ν (Sn–C); 452 ν (Sn–O): **^{1}H NMR** (DMSO-d_6, 400 MHz) δ (ppm): 2.63 (*t*, 2H, H2, ^3J [^{1}H, ^{1}H] = 6.8 Hz); 2.29 (*t*, 2H, H3, ^3J[^{1}H, ^{1}H] = 6.8 Hz); 8.98 (s, 1H NH); 8.36 (d, ^3J[^{1}H, ^{1}H] = 7.6 Hz, 1H, H6); 6.85 (dd, 1H, H8, ^3J[^{1}H, ^{1}H] = 2.4); 7.01 (m, 2H, H7 and H9); 3.77 (s, 3H, H11); {8.66 (d, 1H, ^3J [^{1}H, ^{1}H] = 5.2 Hz); 7.93 (m, 1H); 7.70 (m, 1H); 9.2 (d, 1H, ^3J[^{1}H, ^{1}H] = 5.2 Hz) (2,2′-Bipy H)}; 0.33 (s, 3H, Hα, ^2J[$^{119/117/115}$Sn–^{1}Hα] = 70, 68, 30 Hz): **^{13}C NMR** (DMSO-d_6, 100 MHz) δ (ppm): 176.5 (C1); 33.2 (C2); 31.8 (C3); 171.5 (C4); 128.2 (C5); 121.8 (C6); 120.7 (C7); 124.3 (C8); 111.5 (C9), 149.7 (C10), 56.1 (C11); {149.8, 124.7, 137.8, 121.0, 155.8 (2,2′-Bipy C)}, 0.7 (Cα, ^1J [$^{119/117}$Sn–^{13}Cα] = 521, 500 Hz); **^{119}Sn NMR** (DMSO-d_6, 400 MHz) δ (ppm): −10.1: **ESI-MS**, *m/z* (%): $[C_{24}H_{29}N_3O_4SnNa]^+$, *m/z* = 566 (15); $[C_{24}H_{29}N_3O_4Sn]^+$, *m/z* = 543 (31), $[C_{14}H_{21}NO_4Sn]^+$, *m/z* = 387

(32); $[C_{11}H_{12}NO_4]^+$, m/z = 222 (11); $[C_{10}H_{12}NO_2]^+$, m/z = 178 (12); $[C_3H_9Sn]^+$, m/z = 165 (43); $[C_2H_6Sn]^+$, m/z = 150 (21); $[CH_3Sn]^+$, m/z = 135 (24); $[Sn]^+$, m/z = 120 (5); $[C_{23}H_{26}N_3O_4Sn]^+$, m/z = 528 (13); $[C_{22}H_{26}N_3O_2Sn]^+$, m/z = 484 (10); $[C_{21}H_{23}N_3O_2Sn]^+$, m/z = 469 (8); $[C_{11}H_{15}NO_2Sn]^+$, m/z = 313 (20); $[C_{10}H_{12}NO_2Sn]^+$, m/z = 298 (10); $[C_{10}H_8N_2]^+$, m/z = 157 (100).

2.2.17. (1,10-Phenanthroline) N-[(2-methoxyphenyl)]-4-oxo-4-[(trimethylstannyl)oxy]butanamide (**14**)

Yield: 70%: M.p. 125–127 °C: Mol. Wt.: 566.2: Anal. Calc. for $C_{26}H_{29}N_3O_4Sn$: C, 43.6 (43.7); H, 5.5 (5.1); N, 3.6 (3.2): **IR** (4000–100 cm^{-1}): 3417 ν (NH); 1688 ν (amide C=O); 1519 ν (COOasym); 1393 ν (COOsym); 126 ($\Delta\nu$); 546 ν (Sn–C); 486 ν (Sn–O): **^{1}H NMR** (DMSO-d_6, 400 MHz) δ (ppm): 2.49 (*t*, 2H, H2, ^3J[^{1}H, ^{1}H] = 6.8 Hz); 2.31 (*t*, 2H, H3, ^3J[^{1}H, ^{1}H] = 6.8 Hz); 9.0 (s, 1H NH); 8.18 (d, ^3J[^{1}H, ^{1}H] = 8.4 Hz, 1H, H6); 6.83 (dd, 1H, H8, ^3J[^{1}H, ^{1}H] = 2.4 Hz); 7.04 (m, 2H, H7 and H9); 3.82 (s, 3H, H11); 0.40 (s, 3H, Hα, ^2J[^{119}Sn–^{1}Hα] = 69 Hz); {9.08 (d, 1H, ^3J[^{1}H, ^{1}H] = 5.4 Hz); 7.76 (m, 1H); 8.48 (m, 1H); 7.96 (d, 1H, ^3J[^{1}H, ^{1}H] = 5.4 Hz) (1,10-phen H)}: **^{13}C NMR** (DMSO-d_6, 100 MHz) δ (ppm): 173.5 (C1); 33.0 (C2); 31.7 (C3); 171.4 (C4); 128.2 (C5); 121.9 (C6); 120.7 (C7); 124.3 (C8); 111.5 (C9), 149.7 (C10), 56.1 (C11): 0.4 (Cα, ^1J[^{119}Sn–^{13}Cα] = 525 Hz); {150.5, 123.9, 136.8, 129.0, 145.9, 127.2 (1,10-phen C)}; ^{119}Sn NMR (DMSO-d_6, 400 MHz) δ (ppm): −11.0: **ESI-MS**, m/z (%): $[C_{26}H_{29}N_3O_4SnNa]^+$, m/z = 590 (5); $[C_{26}H_{29}N_3O_4Sn]^+$, m/z = 567 (23); $[C_{14}H_{21}NO_4Sn]^+$, m/z = 387 (22); $[C_{11}H_{12}NO_4]^+$, m/z = 222 (6); $[C_{10}H_{12}NO_2]^+$, m/z = 178 (8); $[C_3H_9Sn]^+$, m/z = 165 (33); $[C_2H_6Sn]^+$, m/z = 150 (13); $[CH_3Sn]^+$, m/z = 135 (17); $[Sn]^+$, m/z = 120 (2); $[C_{25}H_{26}N_3O_4Sn]^+$, m/z = 552 (12); $[C_{24}H_{26}N_3O_2Sn]^+$, m/z = 508 (4); $[C_{23}H_{23}N_3O_2Sn]^+$, m/z = 493 (5); $[C_{11}H_{15}NO_2Sn]^+$, m/z = 313 (13); $[C_{10}H_{12}NO_2Sn]^+$, m/z = 298 (6); $[C_{12}H_7N_2]^+$, m/z = 179 (100); $[C_{12}H_8N_2]^+$, m/z = 180 (9); $[C_{12}H_9N_2]^+$, m/z = 181 (15).

2.3. DNA interaction study assay by UV–visible spectroscopy

SS-DNA (50 mg) was dissolved by overnight stirring in distilled water (pH = 7.0) and kept at 4 °C. 20 mM Phosphate buffer (NaH_2PO_4–Na_2HPO_4, pH = 7.2) was prepared in distilled water. A solution of (SS-DNA) in the buffer gave a ratio of UV absorbance at 260 and 280 nm (A_{260}/A_{280}) of 1.8, indicating that the DNA was sufficiently free of protein [17]. The DNA concentration was determined *via* absorption spectroscopy using the molar absorption coefficient of 6600 M^{-1} cm^{-1} (260 nm) for SS-DNA [18] and was found to be 1.4 × 10^{-4} M. The compound was dissolved in 60% DMSO at a concentration of 1 mM. The UV absorption titrations were performed by keeping the concentration of the compound fixed while varying the SS-DNA concentration. Equivalent solutions of SS-DNA were added to the complex and reference solutions to eliminate the absorbance of DNA itself. Compound-DNA solutions were allowed to incubate for about 10 min at room temperature before measurements were made. Absorption spectra were recorded using cuvettes of 1 cm path length at room temperature (25 ± 1 °C).

2.4. Antibacterial assay

The disc diffusion method [19] was used to check the antibacterial activity of the synthesized compounds against six bacterial strains, namely: *Staphylococcus aureus* (ATCC 6538), *Bacillus subtilis* (ATCC 6633), *Escherichia coli* (ATCC15224), *Bordetella bronchiseptica* (ATCC 4617), *Salmonella typhimurium* (ATCC 14028) and *Enterobacter aerogenes* (ATCC 13048). The organisms were cultured in nutrient broth at 37 °C for 24 h. 1% broth culture containing approx. 10^6 colony-forming units (CFU/mL) of test strain was added to nutrient agar medium at 45 °C and poured into sterile petri plates. The medium was allowed to solidify. 5 μL of the test compound (40 mg/mL in DMSO) was poured on 4 mm sterile paper discs and placed on nutrient agar plates. In each plate DMSO and standard antibacterial drugs (*Roxithromycin* and *Cefixim*) served as negative and positive controls, respectively. Test samples were checked at 200 μg/mL, 100 μg/mL and 50 μg/mL as final concentrations and triplicate plates of each bacterial strain were prepared. The plates were incubated at 37 °C for 24 h and the antibacterial activity was determined by measuring the diameter of zones showing complete inhibition (mm). Growth inhibition was calculated with reference to negative control [20].

2.4.1. Minimum inhibitory concentration (MIC) determination

The MIC (minimum inhibitory concentration) of a bacterium to a certain antimicrobial agent (test compounds) can be determined and today gives the best quantitative estimate for susceptibility. MIC is defined as the lowest concentration of antimicrobial agent required to inhibit growth of the bacteria. The MIC tells about the degree of resistance and might give important information about the resistance mechanism and the resistance genes involved. The principle of MIC determination employing the microdilution method is that after an agar plate is inoculated with the bacteria, a disk or paper strip with antimicrobial agent is placed on the surface. During incubation the antimicrobial agent diffuses into the agar and inhibits growth of the bacteria if sensitive. Diffusion tests are cheap compared to most MIC-determination methods.

Serial twofold dilutions were performed by addition of culture broth to reach concentrations ranging from 200, 100, 50, and 25 μg/mL. The concentration of 100 μg/mL was chosen because it yielded inhibition zones that are wide enough to be measured and sufficiently narrow to be accurately determined. 20 μL of each dilution were distributed in 96-well plates, as well as a sterility control and a growth control (containing culture broth plus DMSO, without antimicrobial substance). Each test and growth control well was inoculated with 5 μL of a bacterial suspension (108 CFU/mL or 105 CFU/well). All experiments were performed in triplicate and the microdilution trays were incubated at 36 °C for 18 h. The results were expressed in micrograms per milliliters [21].

2.5. Antifungal assay

Antifungal activity of the compound was tested against five fungal strains; *Mucor species* (FCBP 0400), *Aspergillus niger* (FCBP 0198), *Aspergillus fumigates* (FCBP 66), *Aspergillus flavous* (FCBP 0064) and *Fusarium solani* (FCBP0291) using the disc diffusion method [21]. The organisms were cultured on SDA at 28 °C for 24 h. Autoclaved broth culture (3 mL) was allowed to cool down to room temperature, poured into sterile Petri plates and the medium was allowed to solidify. Then 5 μL of the test compound (40 mg/mL in DMSO) was poured on 4 mm sterile paper discs and placed on SDA plates. The discs treated with DMSO and *Terbinafine* were used as negative and positive controls, respectively. Plates were incubated at 28 °C for 7 days and fungal growth was determined by measuring growth diameter (mm) around each well. Growth inhibition was calculated with reference to the negative control. The MIC value was noted as lowest concentration at which no growth was observed.

2.6. Brine shrimp lethality assay

The shrimp's lethality bioassay was performed as developed by Michael et al. [22], and later modified by Sleet and Brendel [23]. It was based on the ability to kill laboratory-cultured *Artemia* nauplii (brine shrimp, *Artemia salina*). *Doxorubicin* was used as standard

drug. A stock solution of 40,000 μg/mL of each test compound was prepared by dissolving 40 mg of test compound in 1 mL of DMSO. From this stock solution, further dilutions (0.1 μg/mL, 1 μg/mL and 10 μg/mL) were made by the serial dilution method.

Artificial sea water was prepared using sea salt 34 g/L under constant aeration for 48 h at room temperature. Brine shrimp eggs (Ocean Star Inc., USA) were hatched in shallow rectangular dish (22 × 32 cm) filled with prepared sea water, having a plastic separator of 2 mm in which numerous holes were punched to make two unequal sections in the dish. The eggs (about 25 mg) were sprinkled in the larger section, which was darkened (covered with aluminum foil) whereas the smaller section was illuminated. After 24 h of hatching, phototropic nauplii (brine shrimp larvae) were collected by pipette from the lightened side. From each stock solution (0.1 μg/mL, 1 μg/mL and 10 μg/mL) 25 μL of the test compound was placed in glass vials (25 mL) and 2 mL sea water was added. 15 shrimps were transferred to each vial after counting against light background, using Pasteur pipette, and volume was raised up to 5 mL. The vials were kept under illumination at room temperature (25–28 °C). After 24 h of incubation, surviving shrimps were observed with the help of 3× magnifying glasses. The experiment was performed in duplicate. In case, where control death occurred, the data was corrected using Abbott's formula [24]:

$$\text{Percentage death} = \frac{\text{control} - \text{sample}}{\text{control}} \times 100$$

Then LD_{50} (Lethal Dose that killed 50% of shrimps) was calculated by using Finny software [25].

2.7. Potato disc antitumor assay

Antitumor activity of the synthesized compounds was tested by performing modified potato disc antitumor assay [26,27]. A 48 h old bacterial culture of At-10 strain of *Agrobacterium tumefaciens*, a Gram negative soil bacterium, was used in this experiment. This assay was performed with inoculums at four concentrations of test samples (1000, 100, 10 and 1 μg/mL), containing bacterial culture and 1.5 mL autoclaved distilled water. Red-skinned potatoes were surface sterilized in 0.1% $HgCl_2$ solution, washed three times with autoclaved distilled water, and potato discs of size 8 mm × 4 mm were prepared using a sterilized cork borer. Autoclaved plain agar solution (1.5%) was poured into Petri plates and allowed to solidify. Ten discs were placed on the agar surface of each Petri plate, and 50 μL of inoculum was placed on the surface of each disc. The plates were sealed with parafilm to avoid contamination and moisture loss and were incubated at 28 °C in dark. The experiment was carried out in triplicate and in strict aseptic conditions. After 21 days of incubation, discs were stained with Lugol's solution (10% KI and 5% I_2) and tumors were counted on each disc using dissecting microscope. Percent tumor inhibition was calculated by the following equation [28]:

$$\text{Percent inhibition} = 100 - \left[\frac{\text{Average number of tumors in sample}}{\text{Average number of tumors in negative control}}\right] \times 100$$

2.8. Gel electrophoresis assay

This assay was carried out to check the DNA protection potential of the compound against (OH^-) free radical. The pBR322 plasmid DNA strand breaks were measured by the conversion of super coiled plasmid double-stranded DNA to open circular and linear forms [29,30]. Briefly, the pBR322 plasmid DNA was incubated with the synthesized compounds, $FeSO_4$ and H_2O_2 at 37 °C for 60 min. $FeSO_4$ and H_2O_2 were used as a positive control. The assay was performed at four different concentrations: 1, 10, 100 and 1000 μg/mL. Following incubation, the samples were immediately loaded on a 0.9% agarose gel (used for analysis of intensity of bands), and electrophoresed for 60 min. After electrophoresis, the gels were visualized and photographed. Quantification of closed-circular and nicked DNA was performed using the UVP software. The measurement of intensity of DNA protection of compound against hydroxyl free radical can be explained with the help of following scale.

- (−) sign means DNA damage. No super coiled DNA found
- (+) sign means low DNA protection. Super coiled DNA < open circular DNA with or without linear band.
- (++) sign means mild DNA protection. Super coiled DNA > open circular DNA with or without linear band.
- (+++) sign means good DNA protection. Super coiled DNA > open circular with no linear band.

2.9. Antileishmanial assay

Leishmanial major strain kwh 23 were used for *in vitro* antileishmanial activity. The strains were incubated at 24 °C as previously described by Nabi et al., with a bit modification [31]. The strain was left for 7 days in 199 medium containing 10% Fetal Bovine Serum (PAA Lab, Gmbh). Before starting the activity, stock solutions of 10,000 ppm of the samples were prepared in DMSO. The culture containing about 100 promastigote were transferred to 96 well plates. First row of the 96 well plates contained 198 μL of culture while the remaining wells of the plate contained 180 μL of culture. About 2 μL of the stock solution of each samples was transferred to first row of the plate to obtain a 200 ppm concentration. The concentrations were then serially diluted by transferring 20 μL to each well and then 20 μL were discarded from the last wells. The DMSO concentrations were kept <5% which has no toxic affect on the culture [32]. Negative and positive controls were maintained containing DMSO and drug *Amphotericin B*, respectively. The experiments were repeated 3 times and kept at 24 °C for 72 h. After required time the mortality rates were recorded by transferring 20 μL of the culture to the improved neobar counting chamber under light microscope. For IC_{50} calculation the data were statistically analyzed by Probit regression analysis on SPSS version 16.

3. Results and discussion

3.1. FT-IR spectra

FT-IR data of organotin(IV) derivatives reveal valuable information about the structures of the complexes in the solid state. Comparing the FT-IR spectrum of the free ligands with those of the complexes showed the disappearance of the hydrogen from hydroxyl group at 3200 cm^{-1} indicating the complexation through the oxygen atom. The carboxylate groups in the organotin(IV) derivatives generally adopt a bridged structure in the solid state

unless the organic substituents at tin are bulky or the carboxylate group is branched at the α-carbon [33–35]. The values of $\Delta\nu$ [$\Delta\nu = \nu$ (COOasym) − ν (COOsym)] can be divided into 3 groups; (a) In compounds where $\Delta\nu > 350$ cm^{-1}, the carboxylate group binds in a monodentate fashion. However, other very weak intra- and intermolecular interactions cannot be excluded. (b) When $\Delta\nu < 200$ cm^{-1}, the carboxylate groups of these compounds can be considered to be bidentate. (c) In compounds where $\Delta\nu > 200$ cm^{-1} and <350 cm^{-1} an intermediate state between monodentate and bidentate (anisobidentate) occurs. It has also been suggested that the $\Delta\nu$ value in the chelating mode is less than that in a bridging mode [36,37]. It has been found in literature that when the structure changes from four to five or higher coordinated symmetry, the ν (COOsym) frequencies shift to lower and ν (COOasym) to higher frequencies which cause decrease in the $\Delta\nu$ value in compounds [38]. The magnitude of $\Delta\nu$ for the reported complexes is in the range of 126–202 cm^{-1} which reflects either chelating or bidentate nature of the ligand. Thus, a decrease in the $\Delta\nu$ values are observed in this complex compared to the corresponding free acid. The $\Delta\nu$ value was also calculated from single crystal XRD data for **HL**, complexes **1**, **2**, **3** and **6** by using the following equation [39]:

$$\Delta\nu = 1818.1\delta r + 16.47(\theta\mathrm{OCO} - 120) + 66.8$$

where δr is difference between the two C–O bond lengths (Å) and θOCO is the O–C–O angle (°).

A good correlation was found between the $\Delta\nu$ value calculated from FT-IR data (306, 141, 170, 180 and 202 for **HL**, complexes **1**, **2**, **3** and **6**, respectively) and single crystal XRD data (317, 146, 177, 180 and 208 for HL, complex **2**, **3** and **6**, respectively).

Similarly the appearance of new peaks for ν (Sn–C) in the range of 586–521 cm^{-1} (for alkyl-Sn), 280–267 cm^{-1} (for phenyl-Sn) and for ν (Sn–O) in the range of 481–444 cm^{-1}, respectively confirms the synthesis of the new complexes [40]. The ν (N–H) band in the spectrum of the ligand at 3368 cm^{-1} is also present in the spectra of the complexes in the range of 3434–3368 cm^{-1}.

3.2. Multinuclear (^{1}H, ^{13}C and ^{119}Sn) NMR spectroscopy

3.2.1. ^{1}H and ^{13}C NMR spectroscopy

The ^{1}H NMR studies of compounds provide further support for the formation of compounds. The characteristic peak for the OH bond in the spectrum of the ligand at 12.12 ppm is not present in spectra of the complexes consistent with complexation of the deprotonated ligand to organotin(IV) species through oxygens of carboxylate group. There is no significant change in the position of the NH signal in the spectra of the complexes indicating that nitrogen is not involved in coordination to tin. The phenyl proton at position 6 (H6) appears as a doublet (d) at 7.98 ppm (HL) and from 8.00 to 8.04 ppm in complexes with $^3J(^1\mathrm{H}, ^1\mathrm{H}) = 7.8$ Hz. Proton at position 8 (H8) appears as a doublet of doublets (dd) at 6.91 ppm (HL) and from 6.88 to 6.91 ppm in complexes. Protons at positions 7 and 9 (H7 and H9) appear as a multiplet in the range of 7.08–7.00 ppm. A small upfield shift is observed for protons H7 and H9 which is probably due to the ring current effect.

According to literature, coordination patterns of tin(IV) in di- and tri-methyltin(IV) derivatives with the $^1J[^{119}\mathrm{Sn}-^{13}\mathrm{C}]$ and $^2J[^{119}\mathrm{Sn}-^1\mathrm{H}]$ coupling constant values are as follows: in tetracoordinated tin compounds ^1J values are predicted to be smaller than about 400 Hz, whereas ^2J values should be below 59 Hz; for pentacoordinated tin, ^1J values fall in the range of 450–670 Hz and ^2J values fall in the range of 65–80 Hz; finally, for hexacoordinated tin ^1J and ^2J values are generally larger than 670 and 83 Hz, respectively [41]. Another important parameter that decides the geometry around the tin atom is θ (C–Sn–C angle). Its values are: for tetracoordinated tin compounds, $\theta \leq 112°$, for pentacoordinated tin, $\theta = 115–130°$ and for hexacoordinated tin, $\theta = 129–176°$ [41]. The methyl protons in trimethyltin(IV) complex (**1**) give a characteristic signal at 0.38 ppm with $^2J[^{119/117}\mathrm{Sn}-^1\mathrm{H}] = 70, 68$ Hz which indicates 5-coordinate geometry (trigonal bipyramidal geometry) around the tin atom in solution [41]. The protons of triethyltin(IV) complex (**2**) give two peaks: a quartet for Hα and a triplet for Hβ. In the case of butyl groups, a clear triplet is observed for terminal methyl groups at 0.87 and 0.84 ppm for complexes (**3**) and (**8**), respectively while the protons of other carbon atoms appear as a complex multiplet pattern. The aromatic protons in Ph–Sn appear in the range 7.91–7.15 and 7.90–7.37 ppm, respectively in compounds **4** and **9** [40]. The protons of the cyclohexyl derivatives (complex **5**) give multiplets in aliphatic regions. The methyl protons in the dimethyltin(IV) complex (**7**) give a signal at 0.73 ppm and $^2J[^{119}\mathrm{Sn}-^1\mathrm{H}]$ for dimethyltin(IV) derivatives were found to be 100 Hz that falls in the range of 6-coordinated octahedral geometry. Hα of the benzyl group (complexes **6** and **10**) gives a singlet while the aromatic protons appear in their respective regions. The methyl protons of the *tertiary* butyl group in complex **11**, {C(CH$_3$)$_3$}, appear as a singlet at 1.23 ppm. In case of octyltin(IV) complex (**12**), a somewhat different and complex pattern is observed for the methylene protons. The terminal protons give a triplet while the remaining protons give broad and complex signals.

The ^{13}C NMR data of the ligand and their complexes were in agreement with the ^{1}H NMR and FT-IR data for the formation of complexes. The C1 and C4 of the complexes were shifted downfield compared with the position in the free ligand due to the decrease of electron density at carbon atoms when oxygen is bonded to an electropositive tin atom [40]. This observation provides further evidence that the complexation occurred through the oxygen atoms of the carboxylate group. However, the signals for –C–N–, and –CH$_2$–CH$_2$– peaks for the alkyl as well as aryl groups attached to the tin atom appeared in their specific regions [42]. The positions of the phenyl carbons of ligand undergo minor changes in the complex as compared to those observed in free ligand. In the trimethyltin complex (**1**), the coupling constants $^1J[^{119/117}\mathrm{Sn}-^{13}\mathrm{C}]$ were observed at 523, 400 Hz that fall in the range of 5-coordinate trigonal bipyramidal geometry. This is further supported by the C–Sn–C bond angle (Table 1) calculated from $^1J[^{119}\mathrm{Sn}-^{13}\mathrm{C}]$ value using the Lockhart equation [43] which is for complex **1** is 122.7° that falls in range of 5-coordinated geometry around the tin ($\theta = 115–130°$) [44]. For complex **6** the C–Sn–C bond angle (Table 1) calculated from $^1J[^{119}\mathrm{Sn}-^{13}\mathrm{C}]$ value using the Lockhart equation [43] is 119.2° that is comparable to that observed in single crystal X-ray (119.6°). In case of complex **7**, the C–Sn–C value calculated from $^2J[^{119/117}\mathrm{Sn}-^1\mathrm{H}]$ coupling is 166.2 consistent with 6-coordinate geometry in solution state for diorganotin(IV) derivatives [45]. The *ipso* carbon (Cα) of the phenyl group attached to tin(IV) (complexes **5** and **9**) appears in the range of 5-coordinate

Table 1
(C–Sn–C) angles (°) based on NMR parameters of selected organotin(IV) derivatives.

Comp. no	$^1J(^{119}\mathrm{Sn}, ^{13}\mathrm{C})$ (Hz)	$^2J(^{119}\mathrm{Sn}, ^1\mathrm{H})$ (Hz)	Angle (°)	
			^1J	^2J
1	524	70	123	118
2	490	–	120	–
3	488	–	123	
4	629	–	115	–
5	512	–	121.7	–
6	483	61	119.1	100
7	–	102	–	166
13	521	70	122.5	118
14	525	70	122.9	118

Table 2
Crystal data and structure refinement parameters for HL, **1**, **2**, **3** and **6**.

Parameters	HL	Complex **1**	Complex **2**	Complex **3**	Complex **6**
Empirical formula	$C_{11}H_{13}NO_4$	$C_{14}H_{21}NO_4Sn$	$C_{17}H_{27}NO_4Sn$	$C_{23}H_{39}NO_4Sn$	$C_{32}H_{33}NO_4Sn$
Formula weight	223.22	386.01	428.08	512.24	614.28
Wavelength (λ/Å)	0.71073	0.71073	0.71073	1.5418	0.71073
Temperature/K	296(2)	150(2)	150(2)	190(2)	296(2)
Crystal system	Orthorhombic	Monoclinic	Monoclinic	Monoclinic	Monoclinic
Space group	Pbca	C2/c	$P2_1/c$	$P2_1/n$	$P2_1/n$
a/Å	11.9448(9)	12.473(2)	14.595(4)	18.2080(5)	14.0610(4)
b/Å	10.0633(8)	9.6832(16)	9.877(3)	10.3193(2)	10.6556(3)
c/Å	18.2987(18)	26.208(4)	14.236(4)	27.3873(8)	19.7087(7)
α, β, γ/°	90, 90, 90	90, 100.269(2), 90	90, 115.062(5), 90	90, 98.580(2), 90	90, 101.761(10), 90
Volume/Å^3	2199.6(3)	3114.7(9)	1859.0(10)	5088.3(2)	2890.93(16)
Z	8	8	4	8	4
ρ_{calc}mg/mm^3	1.348	1.646	1.530	1.337	1.411
m/mm^{-1}	0.103	1.652	1.393	8.189	0.920
F(000)	944.0	1552.0	872.0	2128.0	1256.0
Crystal size/mm^3	0.35 × 0.3 × 0.25	0.47 × 0.42 × 0.16	0.17 × 0.09 × 0.03	0.15 × 0.1 × 0.04	0.32 × 0.22 × 0.2
2Θ range for data collection	4.46–52°	3.158–61.144°	3.08–52.434°	6.28–124.56°	3.27–55.694°
Reflections collected	8785	18,215	15,653	27,410	25,738
Independent reflections	2161 [R_{int} = 0.0277, R_{sigma} = 0.0235]	4772 [R_{int} = 0.0514, R_{sigma} = 0.0475]	3714 [R_{int} = 0.1360, R_{sigma} = 0.1138]	8016 [R_{int} = 0.0355, R_{sigma} = 0.0354]	6835 [R_{int} = 0.0340, R_{sigma} = 0.0339]
Data/restraints/parameters	2161/0/148	4772/0/184	3714/0/212	8016/0/523	6832/0/344
Goodness-of-fit on F^2	1.050	1.013	0.986	1.024	1.003
Final R indexes [$I \geq 2\sigma$ (I)]	R_1 = 0.0389, wR_2 = 0.1019	R_1 = 0.0323, wR_2 = 0.0652	R_1 = 0.0601, wR_2 = 0.1106	R_1 = 0.0369, wR_2 = 0.0962	R_1 = 0.0286, wR_2 = 0.0612

geometry [46,47]. The CH_3–Sn signal in complex **7** is broadened and $^1J(^{13}C–^{119}Sn)$ coupling cannot be determined accurately from the spectrum. For complexes **13** and **14** some additional peaks appear in both in ^1H and ^{13}C NMR spectra for 2,2-bipyridine and 1,10-phenanthroline protons and carbons.

3.2.2. ^{119}Sn NMR spectroscopy

^{119}Sn NMR spectroscopy is one of the most potent methods for the study of molecular structure and bonding in organotin compounds. This is due to the wide range of tin chemical shifts and to the strong dependence of tin chemical shifts upon the substituent groups and intermolecular effects [48,49]. The low field displacement of tin chemical shifts in case of complexes **1** (−10.2 ppm), **2** (−18.8 ppm), **3** (−17.6 ppm), **13** (−10.1 ppm), **14** (−11 ppm) is caused by the influence of electron withdrawing and donating ability of the groups attached to ligand as well as electronegativity of the substituent at the tin atom. If the substituent has lone-pair electrons or π electrons of multiple bonds, then an increase in ^{119}Sn shielding will be observed due to the partial filling of the empty *5d* orbital of the tin atom (d–p *or* d_π–p_π interaction). The combination of these competitive effects leads to the tin shielding minimum for the series $Sn(CH_3)_3$, $Sn(C_2H_5)_3$, $Sn(C_4H_9)_3$ [48,49]. The values of ^{119}Sn NMR for complexes **4**, **5** and **6** fall in the normal range of 5-coordinated geometry. In case of diorganotin(IV) derivatives (complexes **7**–**12**) the ^{119}Sn NMR values range from −256.7 ppm to −298.7 ppm falling in the range of 6-coordinate geometry.

Table 3
Selected bond lengths (Å) for HL, **1**, **2**, **3** and **6**.

Bond lengths for HL			
O1–C1	1.305(2)	O2–C1	1.196(2)
C1–C2	1.498(2)	C2–C3	1.522(2)
N1–C4	1.338(2)	N1–C5	1.417(2)
Bond lengths for complex 1			
O-1–Sn1	2.3333(17)	C12–Sn1	2.132(2)
O2–Sn1	2.2149(17)	C13–Sn1	2.128(3)
C1–C2	1.510(3)	C14–Sn1	2.129(2)
C1–O1	1.251(3)	C1–O2	1.271(3)
Bond lengths for complex 2			
O1–Sn1	2.199(6)	C12–Sn1	2.138(3)
O2–Sn1	2.351(6)	C14–Sn1	2.135(9)
C1–C2	1.50(1)	C16–Sn1	2.143(9)
C1–O1	1.28(1)	C1–O2	1.24(1)
Bond lengths for complex 3			
O1–Sn1	2.185(2)	C12–Sn1	2.138(5)
O2–Sn1	2.392(2)	C16–Sn1	2.137(4)
C1–C2	1.505(5)	C20–Sn1	2.128(4)
C1–O1	1.279(4)	C1–O2	1.246(4)
Bond lengths for complex 6			
O1–Sn1	2.156(2)	C19–Sn1	2.149(3)
O2–Sn1	2.451(2)	C12–Sn1	2.138(3)
C1–C2	1.507(3)	C26–Sn1	2.141(2)
C1–O1	1.275(3)	C1–O2	1.230(3)

3.3. X-ray crystallography

Crystal data and structure refinement parameters for all six structures are shown in Table 2 while the selected bond lengths and bond angles are given in Table 3.

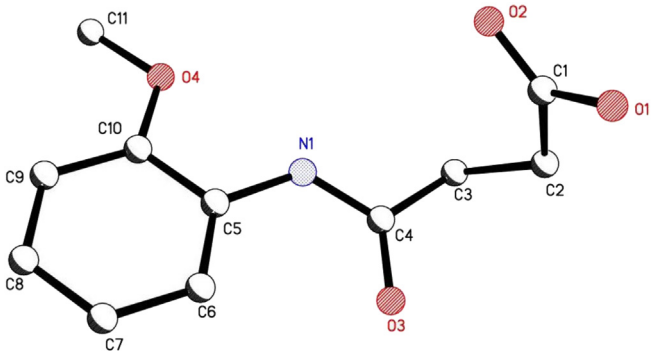

Fig. 1. A perspective view of the **HL** molecule showing the crystallographic numbering scheme. All H-atoms have been omitted for clarity.

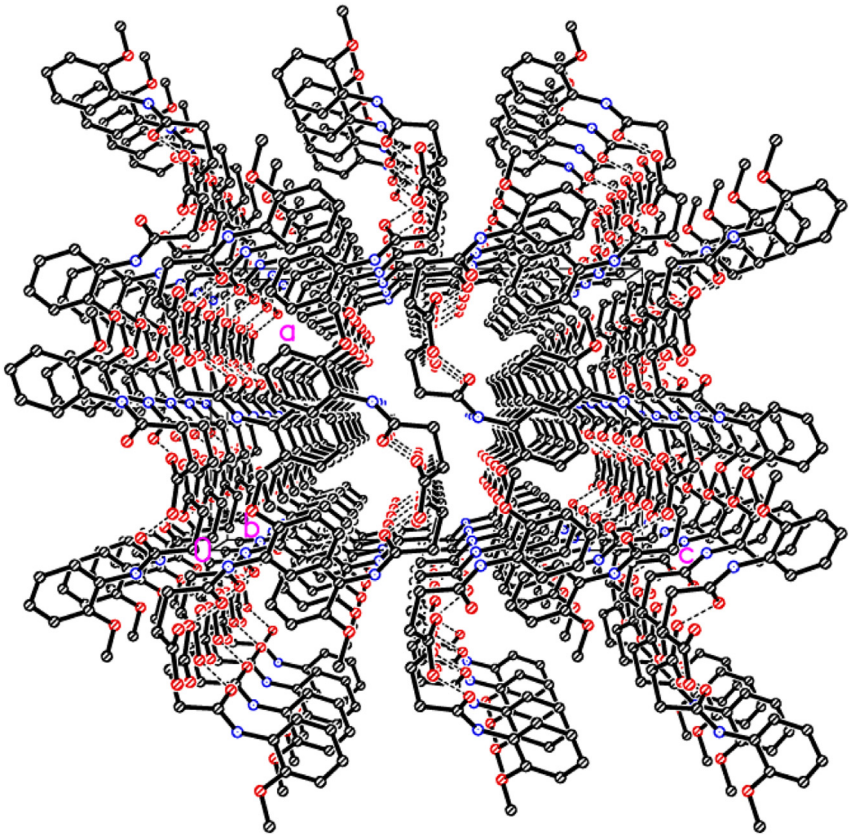

Fig. 2. Packing diagram with unit cell of **HL** viewed along b-axis. Hydrogen bonds are shown as dashed lines and H atoms have been omitted for clarity.

Table 4
Selected bond angles (°) for HL, **1**, **2**, **3** and **6**.

Bond angles for HL			
O1–C1	O1–C1	O1–C1	O1–C1
C1–C2	C1–C2	C1–C2	C1–C2
N1–C4	N1–C4	N1–C4	N1–C4
Bond angles for complex 1			
O1–Sn1–C12	85.43(8)	C12–Sn1–O2	88.26(8)
O1–Sn1–C13	87.58(8)	C13–Sn1–O2	94.22(9)
O1–Sn1–C14	90.01(8)	C14–Sn1–O2	94.13(8)
O1–Sn1–O2	173.57(6)	C12–Sn1–C13	117.28(10)
O1–C1–O2	122.3(2)	C12–Sn1–C14	118.75(10)
O1–C1–C2	120.2(2)	C13–Sn1–C14	123.50(11)
Bond angles for complex 2			
O1–Sn1–C12	93.5(3)	C12–Sn1–O2	90.1(3)
O1–Sn1–C14	91.3(3)	C14–Sn1–O2	83.7(3)
O1–Sn1–C16	93.8(3)	C16–Sn1–O2	86.9(3)
O1–Sn1–O2	174.8(2)	C12–Sn(1)–C14	115.0(3)
O1–C1–O2	122.3(8)	C12–Sn1–C16	128.7(3)
O1–C1–C2	117.0(7)	C14–Sn1–C16	115.5(3)
Bond angles for complex 3			
O1–Sn1–C12	96.6(1)	C12–Sn1–O2	87.8(1)
O1–Sn1–C16	88.6(1)	C16–Sn1–O2	85.4(1)
O1–Sn1–C20	95.6(1)	C20–Sn1–O2	85.8(1)
O1–Sn1–O2	173.8(9)	C20–Sn1–C16	118.7(2)
O1–C1–O2	122.7(3)	C20–Sn1–C12	121.4(2)
O1–C1–C2	116.3(3)	C16–Sn1–C12	118.7(2)
Bond angles for complex 6			
O1–Sn1–C12	95.8(8)	C12–Sn1–O2	88.4(8)
O1–Sn1–C19	96.3(9)	C19–Sn1–O2	90.1(9)
O1–Sn1–C26	91.7(8)	C26–Sn1–O2	77.7(8)
O1–Sn1–O2	169.3(6)	C19–Sn1–C26	118.5(1)
O1–C1–O2	123.6(2)	C12–Sn1–C19	119.5(1)
O1–C1–C2	114.6(2)	C12–Sn1–C26	120.1(1)

3.3.1. HL

N-[(2-methoxyphenyl)]-4-oxo-4-[oxy]butanamide, crystallizes as a monomer in the orthorhombic space group Pbca. The molecular structure is shown in Fig. 1 while its unit cell packing is shown in Fig. 2. Crystal data and structure refinement parameters are shown in Table 2 while selected bond lengths and bond angles are given in Tables 3 and 4, respectively. The conformations of the N–H and the C=O bonds in the amide segment are *anti* to each other. In the side chain, the amide C=O bond is *anti* to the adjacent C–H bond, while the carboxyl C=O bond is *syn* to the adjacent C–H

Table 5
Hydrogen-bond angles and bond lengths (Å,°) for HL, **1**, **2**, **3** and **6**.

D–H···A	D–H	H···A	D···A	D–H···A
HL				
O1–H1···O3^{i}	0.82	1.80	2.606(2)	167.0
N1–H1A···O4	0.86	2.23	2.6028(2)	106.0
C6–H6···O3	0.93	2.28	2.841(2)	118.0
Complex 1				
C11–H11···O3^{i}	0.98	2.41	3.201(4)	137.4
Complex 3				
N1–H1···O4	0.86	2.19	2.606(5)	110.0
N2–H2···O8	0.86	2.17	2.569(6)	108.0
Complex 6				
C6–H6···O3^{i}	0.93	2.30	2.882(4)	120.0

Symmetry transformations used to generate equivalent atoms for HL: (i) 3/2 − x,1/2 + y,+z.
Symmetry transformations used to generate equivalent atoms for complex 1: (i) 1/2 + x,−1/2 + y,+z.
Symmetry transformations used to generate equivalent atoms for complex 6: (i) 1/2 − x,−1/2+y,1/2 − z.

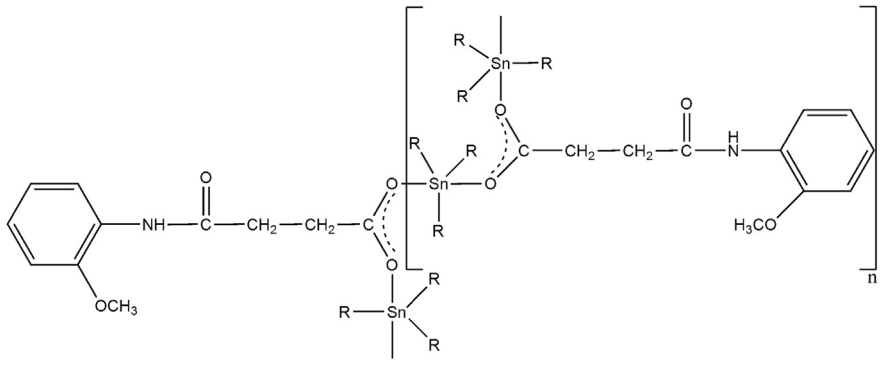

Fig. 3. Polymeric structure of R_3SnL.

bond. The observed rare *anti* conformation of the C=O and O–H bonds of the acid group is similar to that examined in N-(4-Methoxyphenyl)maleamic acid [50]. There is an intramolecular C–H–O and N–H–O interaction within the polymeric chain of the **HL**. An intermolecular C–H–O interaction along b-axis links the polymeric chains in zigzag form (Fig. 2) which are linked into a three-dimensional network *via* C–H–π interactions. The detail of intramolecular H-bonds is given in Table 5.

3.3.2. Complexes *1*, *2*, *3* and *6*

The general polymeric structure of R_3SnL is shown in Fig. 3. The perspective diagrams of the complexes **1**, **2**, **3** and **6** are given in Figs. 4, 6, 8 and 10 while their unit cell packing diagrams are shown in Figs. 5, 7, 9 and 11, respectively. Crystal data and structure refinement parameters are shown in Table 2 while the selected bond lengths and bond angles are given in Tables 3 and 4, respectively. The presence of a bidendate ligand, 4-(2-methoxyphenylamino)-4-oxobutanoate, leads to the formation of the polymeric structure. In other words, the central R_3Sn (R = CH_3, C_2H_5, C_4H_9 and C_7H_7) group bridges the two neighboring 4-(2-methoxyphenylamino)-4-oxobutanoate ligands *via* carboxylate (Fig. 3) moieties to form

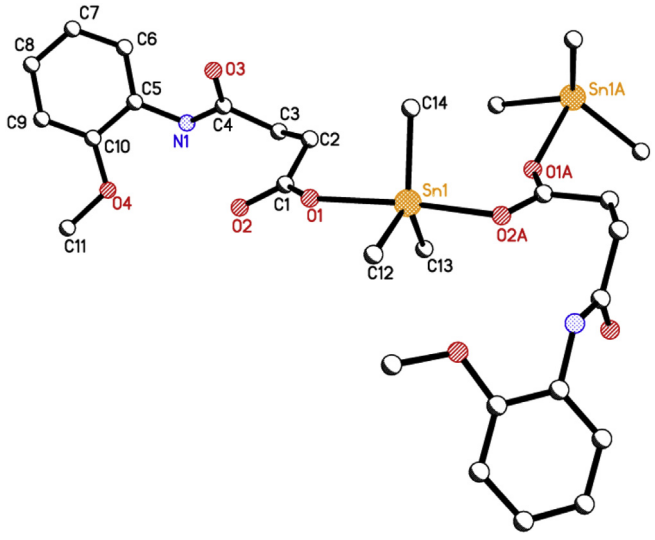

Fig. 4. A perspective view of the complex **1** showing the crystallographic numbering scheme. All H-atoms have been omitted for clarity.

one-dimensional polymeric chain [51]. The geometry around the tin atom is distorted trigonal bipyramidal. The values of τ ($\tau = (\beta - \alpha)/60$, where β is the largest basal angle around the tin atom while α is the next largest angle around the tin atom) for the complexes **1**, **2**, **3**, and **6** are 0.83, 0.80, 0.87 and 0.82, respectively that are typical for distorted trigonal bipyramidal geometry [52]. The geometry around the tin atom is defined by three R groups and two oxygen atoms. The three R groups occupy the equatorial positions with essentially identical bond distances [Sn–C = 2.125–2.149 Å]. The O–Sn–O angle is approximately linear [O–Sn–O = 169.33–174.8°]. The C–Sn–C and O–Sn–C angles are within the expected range of values [C–Sn–C = 115.5(18)°–121.43(19)° and O–Sn–C = 85.40–96.34°] [53]. The sum of the C–Sn–C angles in the equatorial plane equals 359.5°, 359.5°, 359.3° and 358.1°, respectively for complexes **1**, **2**, **3**, **6**, indicating slight distortion. This distortion from ideal trigonal bipyramidal geometry is found in the axial angle [O–Sn–O]. The intramolecular Sn–O1 separation of 2.333(17) Å, 2.199(6) Å, 2.184(3) Å, 2.156(2) Å, respectively for complexes **1**, **2**, **3**, **6** is significantly shorter than the intermolecular Sn–O2 distance of 2.215(17) Å, 2.351(6) Å, 2.392(3) Å, 2.451(2) Å, respectively for complexes **1**, **2**, **3**, **6**. The asymmetric Sn–O separations are reflected in the associated C–O1 and C–O2 distances of 1.251(3) Å, 1.280(1) Å, 1.278(5) Å, 1.257(3) Å and 1.271(3) Å, 1.24(1) Å, 1.246(5) Å, 1.230(3) Å, respectively for complexes **1**, **2**, **3**, **6** [54]. The Sn1–O1, Sn1–O2 (another Sn atom bonded by O2 of the bridging carboxylate ligand) bond distances involving the bridging carboxylate ligand are exactly same indicating a symmetrical bridge. The anisobidentate bidentate carboxylate has a difference of 0.058 Å between its C–O bonds while for the bidentate carboxylate this difference is only 0.021 Å; the variations in the C–O bond distances suggest charge delocalization over the carboxylate group COO. The different modes of bonding of the acetates, i.e., bridging or chelating, are thus easily differentiated by the relevant bond lengths [55]. There is an intramolecular C–H–O (O of amide carbonyl group) interaction within the polymeric chain. An intermolecular C–H–O interaction links the polymeric chains into sheets form (Figs. 7 and 9) or zigzag form (Figs. 5 and 11) which are linked into a three-dimensional network *via* C–H–π interactions. The details of intramolecular H-bonds existing within the structure are given in Table 5.

3.4. Mass spectrometry

The general fragmentation patterns for **HL**, tri- and di-organotin(IV) complexes are shown in Schemes 4–6, respectively. In the mass spectrum of **HL** the molecular ion peak undergoes the elimination of a water molecule generating a mass fragment of *m*/

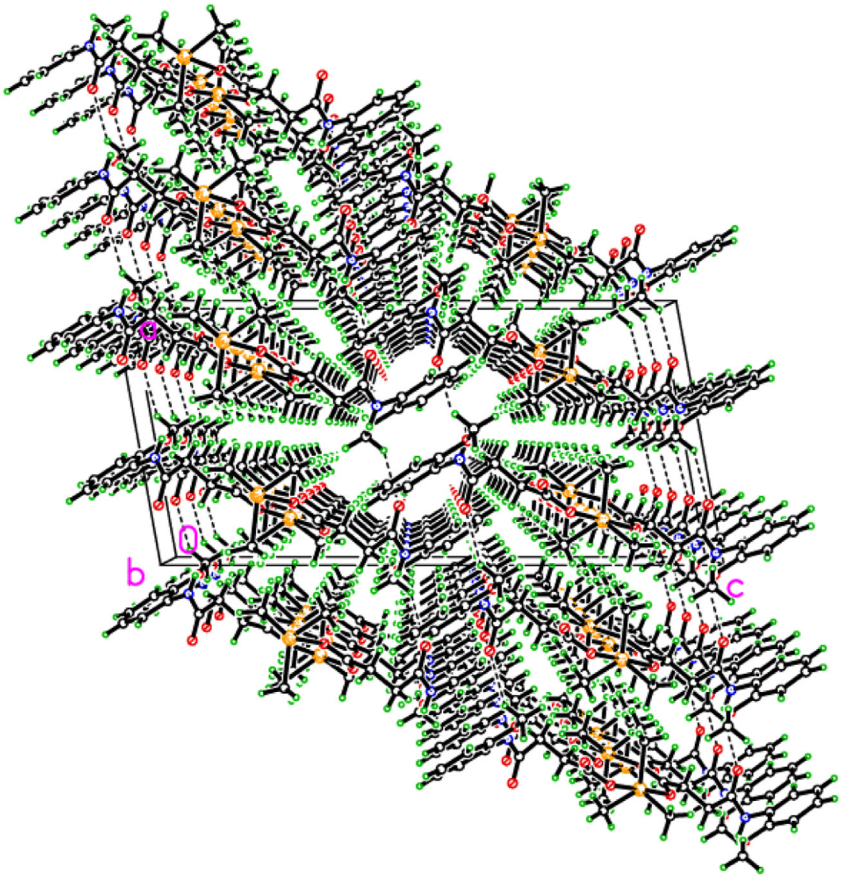

Fig. 5. Packing diagram with unit cell of complex **1** viewed along b-axis.

$z = 205$ that further undergoes the elimination of 2CO and C_2H_2 molecules to give base peak of $m/z = 123$. The base peak undergoes fragmentation in two different ways: in one case it gives a mass fragment of $m/z = 108$ by the elimination of NH fragment while in second way it gives a mass fragment of $m/z = 92$ by the elimination of OCH_3 and H. $[MNa]^+$ fragment of 45% intensity is also observed.

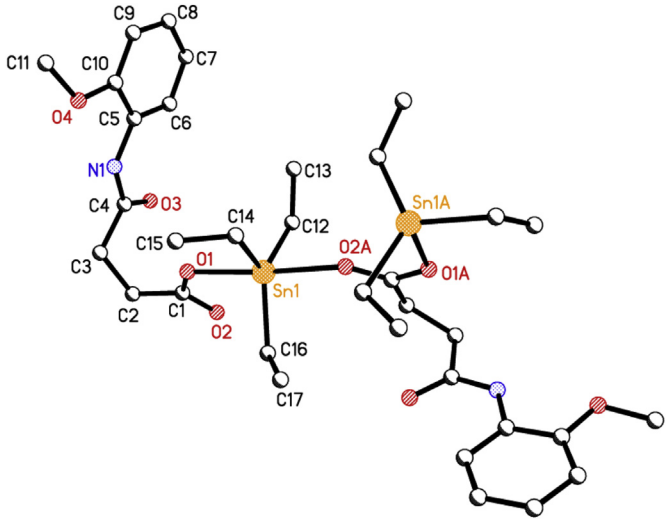

Fig. 6. A perspective view of the complex **2** showing the crystallographic numbering scheme. All H-atoms have been omitted for clarity.

In the mass spectra of all the compounds, each fragment ion occurs in a group of peaks as a result of tin isotopes. For simplicity the mass spectral fragmentation data reported here are related to the principal isotope ^{120}Sn [56]. The low-intensity molecular ion peaks, M^+ were observed in all synthesized organotin carboxylates (**1**–**12**). Also, the $[MNa]^+$ Fragment is observed in all spectra. The fragmented ions are in good agreement with the expected structure of the compounds and consistent with the literature [57,58].

In triorganotin compounds, three primary fragmentation patterns are proposed, based on observed m/z in their spectra. Elimination of different groups like COOR′ and R, gave $[Sn]^+$ as end product in one of the pathways. The other two pathways after primary elimination of $[R]^+$ and $[R_3Sn]^+$ groups and then elimination of COO and successive R (in one of the pathway) results in the formation of $[R']^+$, which shows similar pattern for the further elimination of different groups [59].

A bit different scheme of mass fragmentation pattern has been suggested for the diorganotin compounds but these pathways end up in similar manner as suggested for the triorganotin compounds. In addition, the following ions: $[C_4H_9]^+$, $[C_6H_5]^+$, $[C_7H_7]^+$, and $[C_8H_{17}]^+$ are also observed with reasonable intensities in the mass spectra of all organotin(IV) derivatives [59].

3.5. DNA binding study by UV–visible spectroscopy

Electronic absorption spectra were initially used to examine the interaction between the compounds and SS-DNA. Figs. 12 and 13 (also Figs. S1–S5: Supplementary data) show the UV–visible spectra observed when representative compounds interact with different concentrations of DNA. It was observed that all

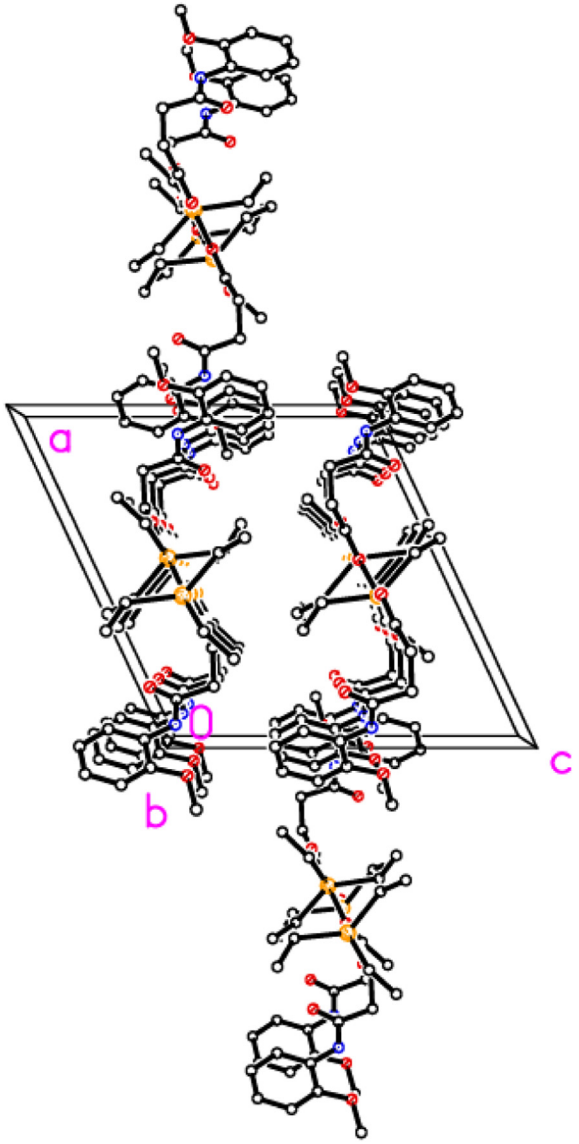

Fig. 7. Packing diagram with unit cell of complex **2** viewed along b-axis.

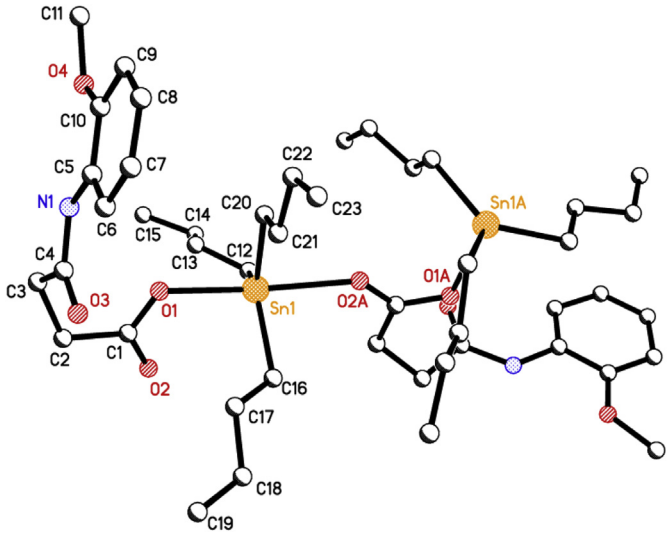

Fig. 8. A perspective view of the complex **3** showing the crystallographic numbering scheme. All H-atoms have been omitted for clarity.

compounds have one strong absorption peak at 280–283 nm. In case of compound **4** a shoulder at 267.40 nm also appeared. After interaction with increasing amounts of DNA, all the peaks decreased gradually and there was a minor red shift of upto 1 nm for all compounds. Long et al. [60], have pointed out that the peak shift of the small molecules after they interacted with DNA could be clues to judge the binding mode between the small molecules and DNA. If the binding involves a typical intercalative mode, an hypochromism (decrease in absorption or molar absorptivity) effect coupled with obvious bathochromism (shift of wavelength toward longer wavelength side, i.e. red shift) for the characteristic peaks of the small molecules will be found due to the strong stacking between the chromophore and the base pairs of DNA [61,62]. Therefore, based on this viewpoint, the interaction between compounds and SS-DNA could be noncovalent intercalative binding. After intercalating the base pairs of DNA, the π^* orbital of the intercalated ligand could couple with π orbital of base pairs, thus decreasing the $\pi-\pi^*$ transition energy, and further resulting in the bathochromism. On the other hand, the coupling of a π orbital with partially filled electrons decreases the transition probabilities hence results hypochromic shift. Since hypochromism due to $\pi-\pi^*$ stacking interactions may appear in the case of the intercalative binding mode, while bathochromism may be observed when the DNA duplex is stabilized [1,63].

Based upon the variation in absorbance, the intrinsic binding constant of the compound with DNA were determined according to Benesi–Hildebrand equation [64]:

$$\frac{A_0}{A-A_0} = \frac{\varepsilon_G}{\varepsilon_{H-G}-\varepsilon_G} + \frac{\varepsilon_G}{\varepsilon_{H-G}-\varepsilon_G} \times \frac{1}{K[DNA]}$$

where K is the association/binding constant, A_0 and A are the absorbances of the compound and its complex with DNA, respectively, and ε_G and ε_{H-G} are the absorption coefficients of the compound and the compound-DNA complex, respectively. The association constants were obtained from the intercept-to-slope ratios of $A_0/(A-A_0)$ *vs.* 1/[DNA] plots. The Gibb's free energy (ΔG) was determined from the equation:

$$\Delta G = -RT \ln K$$

where R is general gas constant (8.314 JK^{-1} mol^{-1}) and T is the temperature (298 K). The binding constants and calculated Gibb's free energies are given in Table 6.

From the interaction study with SS-DNA it is concluded that the synthesized compounds could be used as an anticancer drug.

3.6. Biological activities

3.6.1. Antibacterial activity

In vitro antibacterial screening tests of the synthesized ligand and its organotin(IV) derivatives were carried out against 6 bacterial strains; 2 g-positive [*B. subtilis*, and *S. aureus*] and 4 g-negative [*E. coli*, *B. bronchiseptica*, *S. typhimurium*, *Enterobacter aerogens*]. The disc diffusion method [21,22] was used in this assay and each experiment was performed in triplicate. Readings of the zone of inhibition represent the mean value of 3 readings, which are shown in Table 7. *Roxithromycin* and *Cefixime* were used as standard drugs in these assays. The data obtained show that the synthesized compounds have antibacterial activity. Compounds **1**, **2**, **7**, **11** and **13** have maximum antibacterial activity against all 6 strains. Their activity is

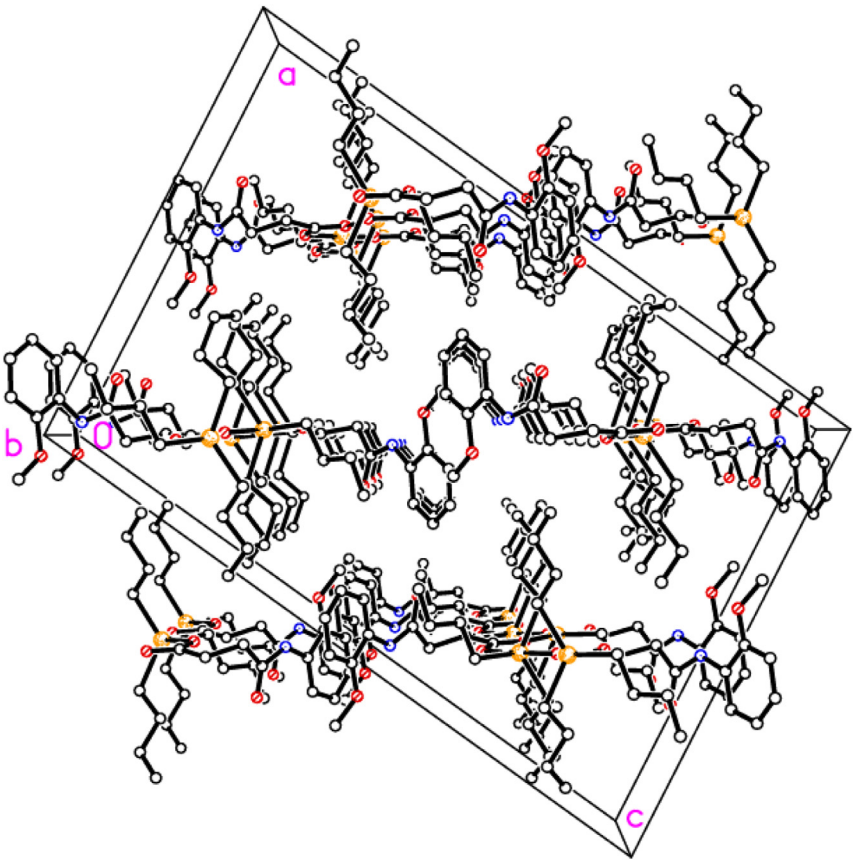

Fig. 9. Packing diagram with unit cell of complex **3** viewed along b-axis.

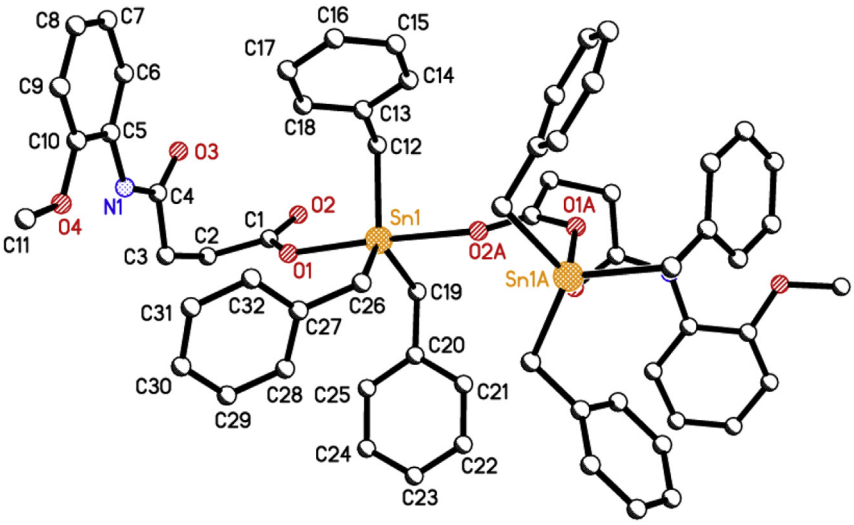

Fig. 10. A perspective view of the complex **4** showing the crystallographic numbering scheme. All H-atoms have been omitted for clarity.

even higher than the standard drugs (*Roxithromycin* and *Cefixime*). Some of the compounds have no activity against some strains but show good activity against the other strains. MIC (minimum inhibitory concentration) values for each compound against each strain are shown in Table 8. The antibacterial activity and inhibition zone around the tested compounds can be caused by their bactericide effects (killing the bacteria) or from their bacteriostatic effects (inhibiting multiplication of bacteria by blocking their active sites on surface or inside bacterial cell). Comparing the biological activity of the ligand and its organotin(IV) complexes with the standard drugs, it is observed that the synthesized compounds have good activity against the studied bacterial strains. A pictorial representation of

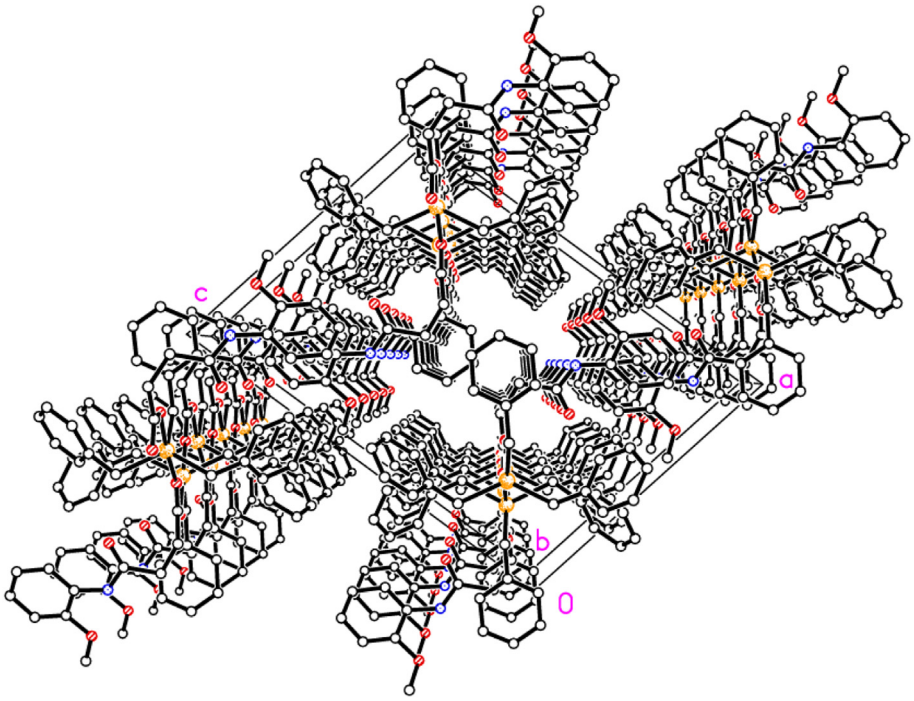

Fig. 11. Packing diagram with unit cell of complex **6** viewed along c-axis.

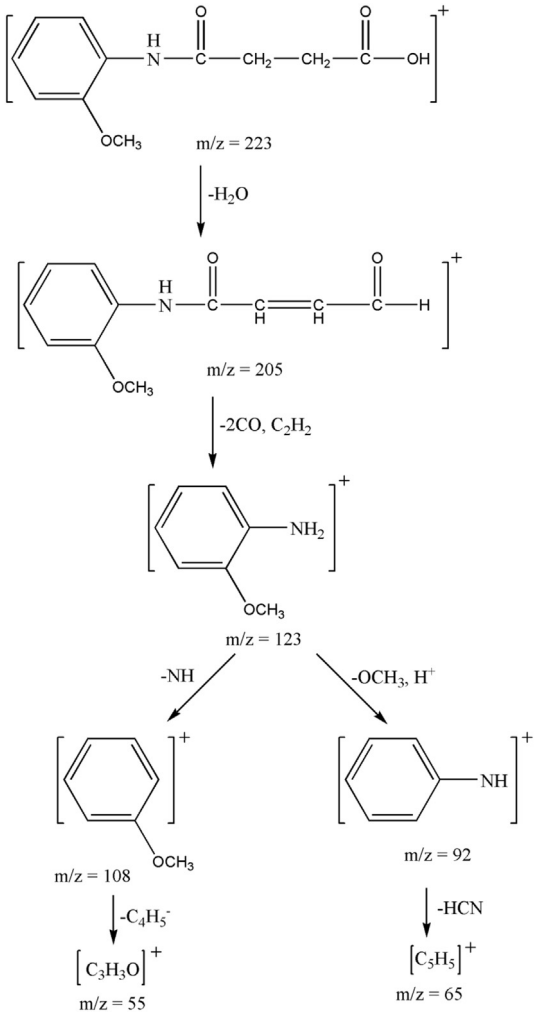

Scheme 4. General fragmentation pattern of HL.

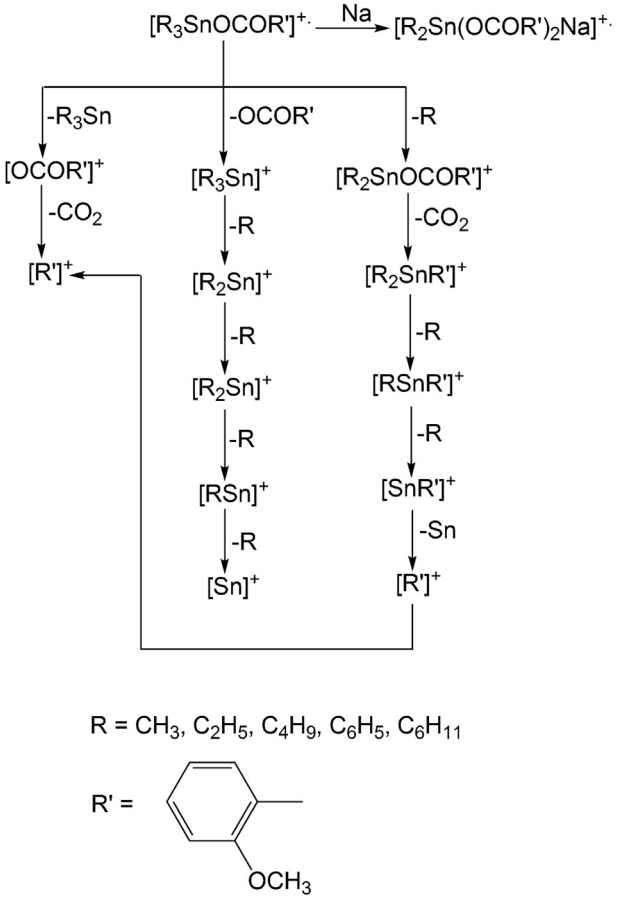

Scheme 5. General fragmentation pattern of triorganotin(IV) complexes.

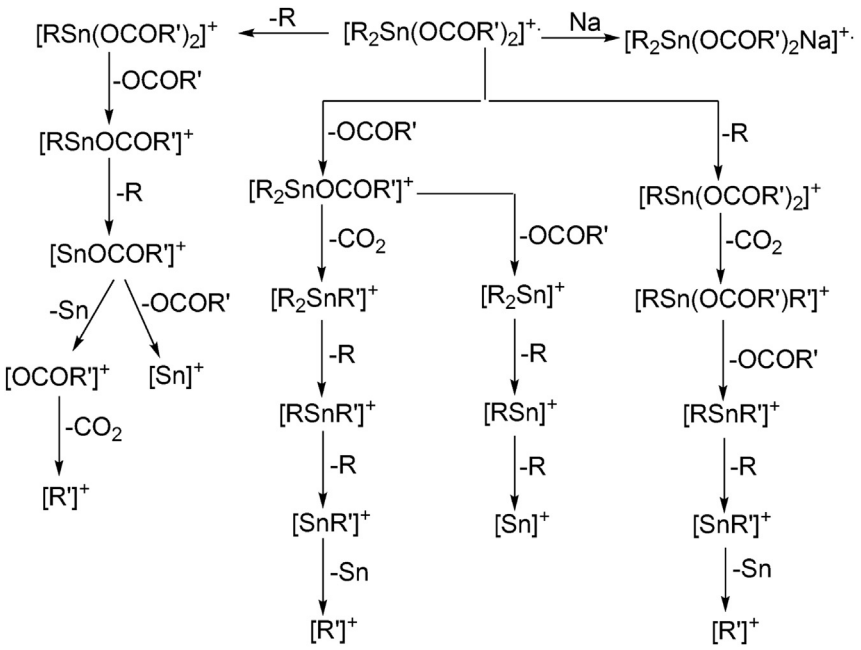

R = CH_3, C_4H_9, C_6H_5, C_8H_{17}, C_2H_3

R' = 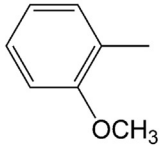

Scheme 6. General fragmentation pattern of diorganotin(IV) complexes.

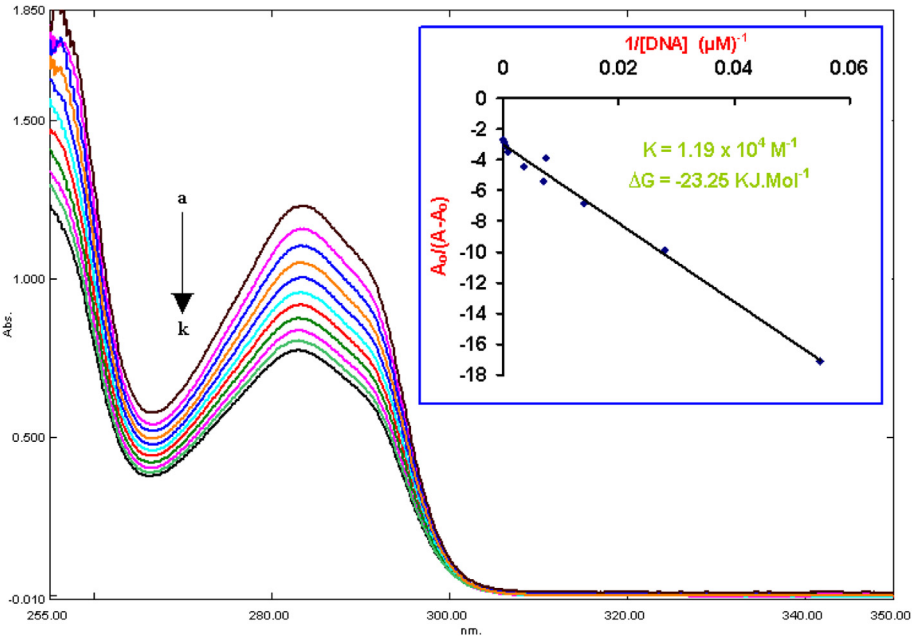

Fig. 12. Absorption spectrum of 1 mM compound **2** in the absence (a) and presence of 9 (b), 18 (c), 27 (d), 36 (e), 45 (f), 54 (g), 63 (h), 72 (i), 81 (j) and 90 (k) μM DNA. The arrow indicates the increasing conc. of DNA. The inset graph represents the plot of $A_o/A - A_o$ *vs.* 1/[DNA] $(\mu M)^{-1}$ for the calculation of binding constant (K) and Gibb's free energy (ΔG).

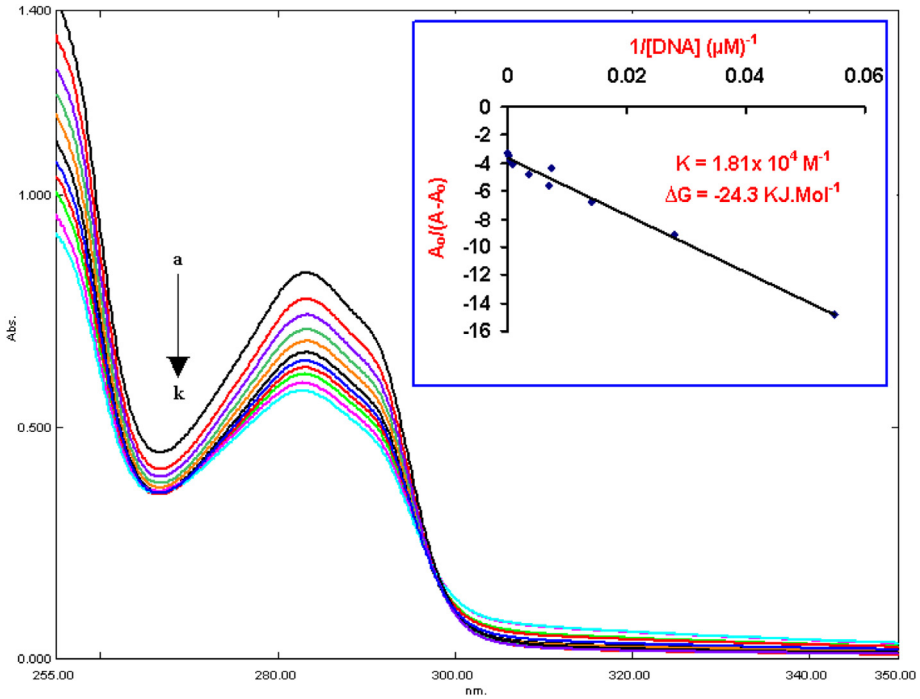

Fig. 13. Absorption spectrum of 1 mM compound **5** in the absence (a) and presence of 9 (b), 18 (c), 27 (d), 36 (e), 45 (f), 54 (g), 63 (h), 72 (i), 81 (j) and 90 (k) μM DNA. The arrow indicates the increasing conc. of DNA. The inset graph represents the plot of $A_o/A - A_o$ *vs.* 1/[DNA] $(\mu M)^{-1}$ for the calculation of binding constant (K) and Gibb's free energy (ΔG).

zone of inhibition of antibacterial activity of one the representative compound is shown in Fig. S6 (supplementary data).

3.6.2. Antifungal activity

All synthesized compounds were also subjected to *in vitro* antifungal activity testing against 4 fungal strains [*Mucor species*, *A. niger*, *Aspergillus flavus* and *Aspergillus fumigatus*] using the disk dilution method [65]. The results are shown in Table 9. Turbinafine was used as the reference drug. All the compounds, except **HL** and **12**, have shown antifungal activity against the various strains. Compound **3** shows higher activity than the reference drug. Their MIC values against each strain are given in Table 10. A pictorial representation of zone of inhibition of antifungal activity of one the representative compound is shown in Fig. S7 (supplementary data). Percentage inhibition and MIC value of biological active samples was evaluated by following formula:

$$\text{Percent inhibition of fungal growth} = \left[\frac{\text{Growth diameter in test compound(mm)}}{\text{Growth diameter in control(mm)}}\right] \times 100$$

Table 6
Overall binding constant and Gibb's free energy data of the selected compounds.[a]

Compound no.	K (M^{-1})	$-\Delta G$ (KJ mol^{-1})
HL	8.26×10^3	22.34
1	9.9×10^3	22.80
2	1.19×10^4	23.25
3	1.24×10^4	23.35
4	1.25×10^4	23.37
5	1.81×10^4	24.3
9	8.7×10^3	22.6
12	3.85×10^3	20.5

[a] Numbering of compounds is in accordance to Scheme 2.

It is concluded from the antibacterial and antifungal activities that some of the synthesized compounds show good antibacterial and antifungal activities even higher than the standards so they can be used as a potent antimicrobial drug.

3.6.3. Cytotoxic activity

This assay is used for preliminary screening which shows cytotoxic effects as well as wide range of pharmacological activities, i.e., pesticidal, anticancer, and antifungal activities [9]. The cytotoxic activity of ligand **HL** and its organotin(IV) complexes (**1**–**14**) were studied *in vitro* against the brine shrimp lethality method by using Doxorubicin as a standard drug and the results are summarized in Table 11. The data is based on mean value of 2 duplicates. The mechanism of toxic effect of organotin(IV) compounds is quite complicated, and it cannot be regarded as thoroughly studied. It is assumed that these compounds are capable of reacting with cell membranes, finally leading to their decay, speed up the ion exchange processes, and inhibiting oxidative and photochemical phosphorylation. Generally, among R_nSnX_{4-n} compounds, the most toxic are the R_3SnX [66]. Toxicity in the R_3Sn series is related to total molecular surface area and to the octanol:water partition coefficient, K_{OW}, which is a measure of hydrophobicity. The high lipid solubility of organotins ensures cell penetration and association with intracellular sites, while cell wall components also play an important role [67]. Also the donor–acceptor interactions between the organotin species and the target organism played an important role in the toxicity mechanism [68]. The brine shrimp cytotoxicity assay is considered as a useful tool for preliminary assessment of toxicity. Cytotoxicity can be considered significant if the LD_{50} value is less than 20–30 μg/mL [69]. Cytotoxic drugs work best in cancers where the cancer cells are rapidly dividing and multiplying. In the present study the LD_{50} value for the tested compounds is less than 4 μg/mL (except compound **12**) so they can be consider as cytotoxic. Thus these compounds can also used for the treatment of cancer.

Table 7
Zone of inhibition (mm) of antibacterial activity of HL and its organotin(IV) derivatives.[a]

Compound no.	*E. coli*	*S. aureus*	*E. aerogens*	*S. typhimurium*	*B. bronchiseptica*	*B. subtilis*
HL	16	11	0	8	9	10
1	26	25	20	23	26	27
2	34	28	22	26	38	36
3	0	12	18	0	12	19
4	0	0	11	0	32	0
5	9	0	0	8	0	0
6	16	17	13	15	13	13
7	16	17	21	16	19	18
8	17	14	27	17	20	22
9	14	16	15	0	11	17
10	16	20	14	0	19	11
11	24	17	40	26	30	40
12	10	0	0	12	11	9
13	16	20	18	28	19	20
14	13	10	14	10	7	16
Cefixime[b]	24	26	10	26	13	25
Roxithromicine[b]	14	14	12	16	19	10

[a] Numbering of compounds is in accordance to Scheme 2.
[b] Reference drugs.

3.6.4. Antitumor activity

The antitumor activity of the synthesized compounds was studied using the potato disc bioassay technique. Minimum inhibitory concentration (MIC) of samples on *A. tumefaciens* are shown in Table 12. The exact mechanism of action is not known but antitumor properties of organotin(IV) compounds are due to inhibition of mitochondrial oxidative phosphorylation (the process of the synthesis of ATP by phosphorylation of ADP for which energy is obtained by electron transport and which takes place in the mitochondria during aerobic respiration) [64,70]. The *A. tumefaciens*-induced potato disc tumor assay is an effective indicator of antitumor activity regardless of the mechanism of drug action. Thus, this assay would be acceptable as a primary general screen for antitumor activity of the synthesized compounds, regardless of mode of inhibitory action on tumor formation. Compounds **2**, **3**, **7**, **8**, **11**, and **13** were found with the highest tumor inhibitions among the tested compounds. A pictorial presentation for one of the representative compound is shown in Fig. S8 (supplementary data). It can be concluded from the DNA interaction, cytotoxicity and antitumor activity that the synthesized compounds might be used as a potent antitumor as well anticancer agent.

3.6.5. Detection of plasmid pBR322 DNA damage by agarose gel electrophoresis

In this assay plasmid pBR322 DNA was used to determine the antioxidant potential of the compound on DNA. The aim of this work was to know the ability of selected organotin(IV) derivatives to unwind or condense a super coiled DNA. The capability of the synthesized compounds to mediate pBR322 DNA damage was investigated using agarose gel electrophoresis at neutral pH and temperature conditions. The mix solution containing compound and DNA were incubated in the presence of $FeSO_4$ and H_2O_2 as a reducing agent for certain time. The electrophorogram of pBR322 DNA damage in presence of different concentrations of the two representative compounds **7** and **1** incubated for 60 min were shown in Fig. 14 while the overall data is shown in Table 13. The treated pBR322 DNA showed two bands on agarose gel electrophoresis. The foremost moving band corresponded to the native

Table 8
MIC values (μg/mL) of antibacterial activity of HL and its organotin(IV) derivatives.[a]

Compound no.	Minimum inhibitory concentration (μg/mL)					
	E. coli	*S. aureus*	*E. aerogens*	*S. typhimurium*	*B. bronchiseptica*	*B. subtilis*
HL	100	100	–	200	200	200
1	25	50	50	25	12.5	25
2	6.25	50	6.25	6.25	6.25	6.25
3	150	150	100	100	100	50
4	–	–	25	–	12.5	–
5	200	–	–	200	–	–
6	50	100	150	200	100	200
7	50	100	100	150	50	100
8	50	100	25	50	50	50
9	25	100	150	–	200	100
10	50	100	150	–	50	200
11	12.5	12.5	6.25	6.25	12.5	12.5
12	200	–	–	150	–	200
13	12.5	50	50	25	100	100
14	150	100	100	200	200	100
Cefixime[b]	–	–	–	–	–	–
Roxithromicine[b]	–	–	–	–	–	–

[a] Numbering of compounds is in accordance to Scheme 2.
[b] Reference drugs.

Table 9
Zone of inhibition (mm) of antifungal activity of HL and its organotin(IV) derivatives.[a]

Compound no.	*A. niger*	*A. fumigates*	*A. flavus*	*M. species*
HL	0	0	0	0
1	28	22	28	24
2	48	58	46	34
3	40	32	32	20
4	40	28	26	23
5	0	16	18	18
6	15	15	12	12
7	15	0	0	0
8	14	12	0	0
9	30	32	26	22
10	11	0	0	0
11	24	18	20	14
12	0	0	0	0
13	26	16	26	0
14	24	16	25	0
Terbinafine[b]	35	35	35	32

[a] Numbering of compounds is in accordance to Scheme 2.
[b] Reference drug.

form of super coiled circular and the slower moving band was the open circular form. Double stranded super coiled structure of plasmid pBR322 DNA with a relatively high electrophoretic mobility is disrupted upon formation of strand breaks, resulting in an open-circle conformation with a reduced electrophoretic mobility in agarose [29,30]. The amount of DNA damage markedly was enhanced with increasing the concentration of the compound (Fig. 14).

3.6.6. Antileishmanial activity

The antiprotozoal activity of the **HL** and its organotin(IV) derivatives against the pathogenic Leishmania was obtained and data are given in Table 14. The synthesized compounds produced a significant reduction in viable promastigotes. The minimum protozoa concentration (IC_{50}) for promastogotes, defined as that concentration which produced 50% reduction in parasites after 72 h of incubation [71]. It is evidenced from the data that the triorganotin(IV) derivatives have higher activity than their diorgano analogues. Potential toxicity, costs, and drug-resistant pathogens necessitate the development of new antileishmanial agents. All the synthesized compounds exhibit strong antileishmanial activity that was even higher than that of amphotericin B with significant cytotoxicity. Their antileishmanial activity may be due the interference with the function of parasite mitochondria. This study, therefore, demonstrated the potential use of these compounds as source of novel agents for the treatment of leishmaniasis.

Table 10
MIC values (μg/mL) of antifungal activity of HL and its organotin(IV) derivatives.[a]

Compound no.	Minimum inhibitory concentration (μg/mL)			
	A. niger	*A. fumigates*	*A. flavus*	*M. species*
HL	–	–	–	–
1	12.5	50	50	50
2	0.78	0.78	0.78	12.5
3	1.56	3.12	3.12	12.5
4	3.12	6.25	6.25	25
5	200	150	150	100
6	150	150	200	200
7	200	–	–	–
8	150	200	–	–
9	1.56	6.25	6.25	100
10	200	–	–	–
11	100	100	100	200
12	–	–	–	–
13	50	100	100	200
14	100	150	50	200

[a] Numbering of compounds is in accordance to Scheme 2.

Table 11
Cytotoxicity data of HL and its organotin(IV) derivatives.[a]

Compound no.	No. of shrimps killed out of 30 per dilution[b]					LD_{50} (μg/mL)
	200 ppm	66.6 ppm	22.2 ppm	7.4 ppm	2.4 ppm	
HL	16	13	12	11	9	192.2
1	30	30	27	24	21	1.09
2	30	30	30	30	28	0.881
3	30	30	30	28	26	0.433
4	30	30	30	29	25	0.793
5	30	30	30	30	29	0.493
4	30	30	30	28	26	0.793
7	27	26	21	18	13	2.89
8	30	30	28	26	23	0.611
9	30	30	28	26	25	0.403
10	30	30	30	30	27	1.105
11	30	27	24	20	14	3.114
12	21	23	20	17	20	6.19
13	30	30	30	27	22	1.17
14	30	30	28	25	24	0.499
Doxorubicin[c]	30	30	27	25	24	0.434
Vehicle control	–	–	–	–	–	–

[a] Numbering of compounds is in accordance to Scheme 2.
[b] Against brine-shrimps (*in vitro*).
[c] Standard drug.

4. Conclusions

The ligand, N-[(2-methoxyphenyl)]-4-oxo-4-[oxy]butanamide, coordinates to tin *via* oxygen atoms of the carboxylate group. In the case of triorganotin(IV) derivatives the geometry around the tin atom is distorted trigonal-bipyramidal both in solution and solid states. While in case of diorganotin(IV) derivatives the geometry around the tin atom is octahedral. A good correlation was found between the $\Delta\nu$ value calculated from FT-IR data and single crystal XRD data. From the single crystal X-ray structural analysis it is revealed that these compounds have packing diagrams like dendrimers with characteristics that make them useful for numerous biological applications. Biological studies reveal that generally the triorganotin(IV) complexes have higher activity than their

Table 12
Potato disc antitumor data of HL and its organotin(IV) derivatives.[a]

Compound no.	Percentage inhibition ± standard deviation			IC_{50} μg/mL
	1000 μg/mL	100 μg/mL	10 μg/mL	
HL	62.64 ± 0.27	31.14 ± 0.40	5.63 ± 0.24	410.37
1	69.88 ± 0.17	54.82 ± 0.26	30.22 ± 0.23	82.24
2	84.14 ± 0.17	70.33 ± 0.29	48.26 ± 0.20	13.52
3	87.82 ± 0.17	72.39 ± 0.20	52.28 ± 0.40	10.35
4	77.47 ± 0.14	54.94 ± 0.24	32.18 ± 0.26	59.29
5	80.91 ± 0.29	57.35 ± 0.23	36.55 ± 0.32	40.77
6	76.12 ± 0.23	62.0 ± 0.17	20.32 ± 0.26	60.34
7	91.37 ± 0.26	62.87 ± 0.18	43.21 ± 0.24	21.70
8	88.27 ± 0.20	65.51 ± 0.23	50.22 ± 0.32	12.28
9	85.28 ± 0.26	62.18 ± 0.20	43.90 ± 0.23	21.36
10	87.12 ± 0.23	52.0 ± 0.17	19.31 ± 0.26	83.24
11	92.41 ± 0.15	71.49 ± 0.08	53.44 ± 0.28	8.78
12	65.47 ± 0.14	44.94 ± 0.24	31.18 ± 0.26	69.25
13	84.82 ± 0.25	66.66 ± 0.23	46.78 ± 0.29	14.77
14	66.68 ± 0.23	45.63 ± 0.42	27.12 ± 0.31	72.87
Vincristine[b]	100	100	100	

[a] Numbering of compounds is in accordance to Scheme 2.
[b] Reference drug.

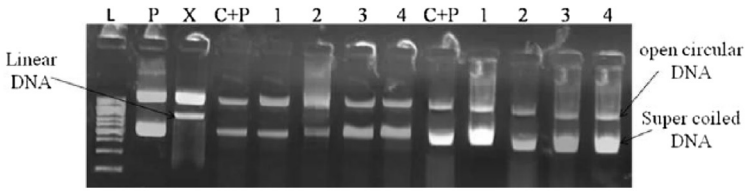

L = DNA ladder (1 kb). P = Plasmid (pBR322) DNA. X = Plasmid with $FeSO_4$ and H_2O_2 (positive control). C+P = Plasmid + 1000 μg/mL of compound **7**: control for pro- oxidant effect of compound on DNA. 1 = Plasmid + 1000 μg/mL of compound **7** + $FeSO_4$ + H_2O_2. 2 = Plasmid + 100 μg/mL of compound **7** + $FeSO_4$ + H_2O_2. 3 = Plasmid + 10 μg/mL of compound **7** + $FeSO_4$ + H_2O_2. 4 = Plasmid + 1 μg/mL of compound **7** + $FeSO_4$ + H_2O_2. C+P = Plasmid + 1000 μg/mL of compound **1**: control for pro- oxidant effect of compound on DNA. 1 = Plasmid + 1000 μg/mL of compound **1** + $FeSO_4$ + H_2O_2. 2 = Plasmid + 100 μg/mL of compound **1** + $FeSO_4$ + H_2O_2. 3 = Plasmid + 10 μg/mL of compound **1** + $FeSO_4$ + H_2O_2. 4 = Plasmid + 1 μg/mL of compound **1** + $FeSO_4$ + H_2O_2.

Fig. 14. Effects of compounds **7** and **1** on plasmid (pBR322) DNA.

Table 13
Plasmid pBR322 DNA damage by agarose Gel Electrophoresis data.[a]

Compound no.	DNA protection activity at different concentration			
	1000 μg/mL	100 μg/mL	10 μg/mL	1 μg/mL
HL	–	–	–	–
1	+++	+++	++	++
2	+	+	+	+
3	–	–	–	–
4	+++	++	+	+
5	–	–	–	–
6	++	++	++	+
7	+++	+++	+++	++
8	–	–	–	–
9	++	++	+	+
10	+	+	++	++
11	++	++	+	+
13	–	–	–	–
14	+++	++	++	+

(–) = no protection, (+) = Slight protection, (++) = Moderate protection, (+++) = Good protection.
[a] Numbering of compounds is in accordance to Scheme 2.

Table 14
Antileishmanial data of HL and its organotin(IV) derivatives[a].

Compound no.	IC_{50} (μg/mL)
HL	3.42×10^{-3}
1	7.59×10^{-5}
2	9.19×10^{-5}
3	4.17×10^{-5}
4	8.70×10^{-5}
5	3.90×10^{-5}
6	9.96×10^{-5}
7	5.89×10^{-4}
8	6.65×10^{-4}
9	6.60×10^{-4}
10	7.96×10^{-4}
11	1.92×10^{-3}
12	1.04×10^{-3}
13	1.56×10^{-2}
14	9.22×10^{-2}
Amphotericin B[b]	0.56

[a] Numbering of compounds is in accordance to Scheme 2.
[b] Reference drug.

corresponding diorganotin(IV) complexes, possibly due to their greater lipophilicity and permeability through the cell membrane. The high lipid solubility of organotins ensures cell penetration and association with intracellular sites. In solution, triorganotin compounds may undergo spontaneous disproportionation into the corresponding diorganotin and tetraorganotin derivatives while, *in vivo*, the loss of one alkyl or aryl group may occur through the intervention of enzymes such as aromatase. UV–Vis spectroscopic results show that the synthesized compounds bind to DNA *via* intercalative mode of interaction resulting in hypochromism and minor red shift. The synthesized compounds may represent a new line of antitumor agents for prevention and treatment of cancer and also serve as a potential source of chemoprotective agent(s). The oxidative DNA damage by the synthesized compounds in the presence of $FeSO_4$ and H_2O_2 (used as a positive control) was explored using agarose gel electrophoresis. The extent of pBR322 DNA damage was enhanced significantly with increasing concentration of the compounds. The antileishmanial data clearly indicate that these compounds have a strong antileishmanial activity and might be developed a new antileishmanial drug. Their antileishmanial activity may be due the interference with the function of parasite mitochondria.

Acknowledgment

Muhammad Sirajuddin gratefully acknowledges the Higher Education Commission (HEC) Islamabad, Pakistan, for financial support (PIN#117-7338-PS7-017).

Appendix A. Supplementary data

Supplementary data related to this article can be found at http://dx.doi.org/10.1016/j.ejmech.2014.07.028.

References

[1] M. Sirajuddin, S. Ali, A. Haider, N.A. Shah, A. Shah, M.R. Khan, Polyhedron 40 (2012) 19–31.
[2] M.S. Ahmad, M. Hussain, M. Hanif, S. Ali, M. Qayyum, B. Mirza, Chem. Biol. Drug. Des. 71 (2008) 568–576.
[3] M. Sirajuddin, S. Ali, F.A. Shah, M. Ahmad, M.N. Tahir, J. Iran. Chem. Soc. 11 (2013) 297–313.
[4] S.K. Hadjikakou, N. Hadjiliadis, Coord. Chem. Rev. 253 (2009) 235–249.

[5] C. Pellerito, P.D. Agati, T. Fiore, C. Mansueto, V. Mansueto, G. Stocco, L. Nagy, Pellerito, J. Inorg. Biochem. 99 (2005) 1294–1305.
[6] P.J. Blower, Annu. Rep. Prog. Chem. Sect. A 100 (2004) 633–658.
[7] F. Barbieri, M. Viale, F. Sparatore, G. Schettini, A. Favre, C. Bruzzo, F. Novelli, A. Alama, Anti-cancer Drugs 13 (2002) 599–604.
[8] X. Shang, X. Meng, E.C.B.A. Alegria, Q. Li, M.F.C. Guedes da Silva, M.L. Kuznetsov, A.J.L. Pombeiro, Inorg. Chem. 50 (2011) 8158–8167.
[9] M. Tariq, N. Muhammad, M. Sirajuddin, S. Ali, N.A. Shah, N. Khalid, M.R. Khan, M.N. Tahir, J. Organomet. Chem. 723 (2013) 79–89.
[10] C. Pellerito, L. Nagy, L. Pellerito, A. Szorcsik, Chem. 691 (2006) 1733–1747.
[11] M. Nath, S. Pokharia, G. Eng, X. Song, A. Kumar, J. Organomet. Chem. 669 (2003) 109–123.
[12] W.L.F. Armarego, C.L.L. Chai, Purification of Laboratory Chemicals, fifth ed., Butterworth-Heinemann, London, New York, 2003.
[13] K. Sisido, Y. Takeda, Z. Kingawa, J. Am. Chem. Soc. 83 (1961) 538–541.
[14] G.M. Sheldrick, Acta Crystallogr. A64 (2008) 112–122.
[15] G.M. Sheldrick, University of Göttingen, Germany, 2012.
[16] F.A. Shah, M. Sirajuddin, S. Ali, S.M. Abbas, M.N. Tahir, C. Rizzoli, Inorgan. Chim. Aca 400 (2013) 159–168.
[17] M. Sirajuddin, S. Ali, N.A. Shah, M.R. Khan, M.N. Tahir, Spectrochim. Acta Part A 94 (2012) 134–142.
[18] M. Sirajuddin, S. Ali, A. Badshah, J. Photochem. Photobiol. B 124 (2013) 1–19.
[19] A. Felten, B. Grandry, P.H. Langrange, I. Casin, J. Clin. Microbiol. 40 (2002) 2766–2771.
[20] L. Jafri, F.L. Ansari, M. Jamil, S. Kalsoom, S. Qureishi, B. Mirza, Chem. Biol. Drug. Des. 79 (2012) 950–959.
[21] S. Arikan, V. Paetznick, J.H. Rex, Antimicrob. Agents Chemother. 46 (2002) 3084.
[22] A.S. Michael, C.G. Thompson, M. Abramovitz, Science 123 (1956) 464.
[23] R.B. Sleet, K. Brendel, Ecotoxicol. Environ. Saf. 7 (1983) 435–446.
[24] W.S. Abbott, J. Econ. Entomol. 18 (1925) 265–267.
[25] D.J. Finney, Probit Analysis, third ed., Cambridge University Press, Cambridege, 1971, p. 333.
[26] A. Ullah, F.L. Ansari, I. Haq, S. Nazir, B. Mirza, Chem. Biodivers. 4 (2007) 203–214.
[27] J.L. McLaughlin, Methods in Plant Biochemistry, Academic Press, London, 1991, p. 1.
[28] S. Kanwal, N. Ullah, I. Haq, I. Afzal, B. Mirza, Pak. J. Bot. 43 (2011) 85–89.
[29] Y. Wang, X. Zhang, Q. Zhang, Z. Yang, Biometals 23 (2010) 265–273.
[30] B. Tian, Y. Hua, Food Chem. 91 (2005) 413–418.
[31] S. Nabi, N. Ahmed, M.J. Khan, Z. Bazai, M. Yasinzai, Y.M.S.A. Al-Kahraman, World Appl. Sci. J. 19 (2012) 1495–1500.
[32] L. Zhai, M. Chen, J. Blom, T.G. Theander, S.B. Christensen, A. Kharazmi, J. Antimicrob. Chemother. 43 (1999) 793–803.
[33] M. Vornefeld, F. Huber, H. Preut, G. Ruisi, R. Barbieri, Appl. Organomet. Chem. 6 (1992) 75–82.
[34] K. Shahid, S. Shahzadi, S. Ali, J. Serbian Chem. Soc. 74 (2009) 141–154.
[35] A. Hameed, T. Mohamad, E. Saad, Y. Farina, A. Graisa, E. Yousif, Eur. J. Sci. Res. 34 (2009) 212–217.
[36] G. Eng, X. Song, A. Zapata, A.C. de Dios, L. Casabianca, R.D. Pike, J. Organomet. Chem. 692 (2007) 1398–1404.
[37] G.K. Sandhu, R. Hunda, E.R.T. Tiekink, J. Organomet. Chem. 430 (1992) 15–23.
[38] D. Kovala-Demertzi, V.N. Dokorou, J.P. Jasinski, A. Opolski, J. Wiecek, M. Zervou, M.A. Demertzis, J. Organomet. Chem. 690 (2005) 1800–1806.
[39] V. Zelenak, Z. Vargova, K. Gyoryova, Spectrochim. Acta Part A 66 (2007) 262–272.
[40] Y. Farina, A. Graisa, E. Yousif, Mod. Appl. Sci. 3 (2009) 215–218.
[41] T.P. Lockhart, W.F. Manders, Inorg. Chem. 25 (1986) 892–895.
[42] B. Wrackmeyer, Annu. Rep. NMR Spectrosc. 38 (1999) 203–264.
[43] T.P. Lockhart, W.F. Manders, E.M. Holts, J. Am. Chem. Soc. 108 (1986) 6611–6616.
[44] G. Casella, F. Ferrante, G. Saielli, Inorg. Chem. 47 (2008) 4796–4807.
[45] H. Jankovics, L. Nagy, Z. Kele, C. Pettinari, P. D'Agati, C. Mansueto, C. Pellerito, L. Pellerito, J. Organomet. Chem. 668 (2003) 129–139.
[46] A. Lycka, M. Nadvornik, K. Handlir, J. Holecek, Collect. Czech. Chem. Commun. 49 (1984) 2903–2911.
[47] R. Willem, A. Bouhdid, M. Biesemans, J.C. Martins, D. Vos, E.R.T. Tiekink, M. Gielen, J. Organomet. Chem. 514 (1996) 203–212.
[48] V.N. Torocheshnikov, A.P. Tupciauskas, A.Y.A. Ustynyuk, J. Organomet. Chem. 81 (1974) 351–356.
[49] J.J. Burke, P.C. Lauterbur, J. Am. Chem. Soc. 83 (1961) 326–331.
[50] B.T. Gowda, M. Tokarcik, K. Shakuntala, J. Kozisek, H. Fuess, Acta Crystallogr. E66 (2010) O1529.
[51] A.W. Addison, R.T. Nageswara, J. Reedijk, J. Van Rijn, G.C. Verschoor, J. Chem. Soc. Dalt. Trans. (1984) 1349–1356.
[52] M.N. Tahir, D. Ulku, M. Danish, S. Ali, A. Badshah, M. Mazhar, Acta Crystallogr. C53 (1997) 183–185.
[53] Sadiq-ur-Rehman, S. Ali, M. Mazhar, M. Parvez, Acta Crystallogr. E60 (2004) m1394–m1396.
[54] T.S.B. Baul, E.R.T. Tiekink, Acta Crystallogr. C52 (1996) 1428–1430.
[55] V. Dokorou, M.A. Demertzis, J.P. Jasinski, D. Kovala-Demertzi, J. Organomet. Chem. 689 (2004) 317–325.
[56] Sadiq-ur-Rehman, K. Shahid, S. Ali, M.H. Bhatti, M. Parvez, J. Organomet. Chem. 690 (2005) 1396–1408.
[57] M.H. Bhatti, S. Ali, M. Mazhar, M. Danish, M.A. Choudhary, Turk. J. Chem. 23 (1999) 329–337.
[58] S. Shahzadi, K. Shahid, S. Ali, M.H. Bhatti, J. Chem. Soc. Pak. 26 (2004) 395–399.
[59] Sadiq-ur-Rehman, M.A. Choudhary, M.H. Bhatti, S. Ali, J. Iran. Chem. Soc. 9 (2012) 35–45.
[60] E.C. Long, J.K. Barton, Chem. Res. 23 (1990) 271–273.
[61] Q. Wang, X. Wang, Z. Yu, X. Yuan, K. Jiao, Int. J. Electrochem. Sci. 6 (2011) 5470–5481.
[62] M. Hossain, M.F. Aziz, R. Ahmed, M. Hossain, A. Mahmuda, T. Ahmed, M.H. Mazumder, Int. J. Pharm. Pharm. Sci. 2 (2010) 60–63.
[63] M. Sirajuddin, N. Uddin, S. Ali, M.N. Tahir, Spectrochim. Acta Part A 116 (2013) 111–121.
[64] H.A. Benesi, J.H. Hildebrand, J. Am. Chem. Soc. 71 (1949) 2703–2707.
[65] A. Rehman, M.I. Choudhary, W.J. Thomsen, Bioassay Techniques for Drug Development, Harwood Academic Publishers, Amsterdam, The Netherlands, 2001, p. 9.
[66] S. Tabassum, C. Pettinari, J. Organomet. Chem. 691 (2006) 1761–1766.
[67] A.K. Saxena, Appl. Organomet. Chem. 1 (1987) 39–56.
[68] Y. Baravalia, Y. Vaghasiya, S. Chanda, Iran. J. Pharm. Res. 11 (2012) 851–861.
[69] A.J. Crowe, P.J. Smith, G. Atassi, Inorg. Chim. Acta 93 (1984) 179–184.
[70] F. Hadizadeh, A. Moradi, G. Naghibi, M. Vojdani, J. Behravan, M. Ramezani, Int. J. Biomed. Sci. 3 (2007) 60–64.
[71] S. Shahzadi, S. Ali, K. Shahid, M. Yousaf, S.K. Sharma, K. Qanungo, J. Chin. Chem. Soc. 57 (2010) 659–670.